

Resolution of the ATLAS muon spectrometer monitored drift tubes in LHC Run 2



The ATLAS collaboration

E-mail: atlas.publications@cern.ch

ABSTRACT: The momentum measurement capability of the ATLAS muon spectrometer relies fundamentally on the intrinsic single-hit spatial resolution of the monitored drift tube precision tracking chambers. Optimal resolution is achieved with a dedicated calibration program that addresses the specific operating conditions of the 354 000 high-pressure drift tubes in the spectrometer. The calibrations consist of a set of timing offsets and drift time to drift distance transfer relations, and result in chamber resolution functions. This paper describes novel algorithms to obtain precision calibrations from data collected by ATLAS in LHC Run 2 and from a gas monitoring chamber, deployed in a dedicated gas facility. The algorithm output consists of a pair of correction constants per chamber which are applied to baseline calibrations, and determined to be valid for the entire ATLAS Run 2. The final single-hit spatial resolution, averaged over 1172 monitored drift tube chambers, is $81.7 \pm 2.2 \mu\text{m}$.

KEYWORDS: Gaseous detectors; Muon spectrometers; Particle tracking detectors (Gaseous detectors); Wire chambers (MWPC, Thin-gap chambers, drift chambers, drift tubes, proportional chambers etc)

ARXIV EPRINT: [1906.12226](https://arxiv.org/abs/1906.12226)



Contents

1	Introduction	1
2	ATLAS detector	2
3	Analysed data	3
4	MDT calibration	4
4.1	Drift radius determination	4
4.2	t_0 determination	4
4.3	$R(t)$ function determination	5
4.4	Gas monitor chamber	6
4.5	Residuals and resolution	7
5	Correction algorithms	8
5.1	δt_0 correction	8
5.2	δP correction	10
6	Resolution results	13
7	Systematic uncertainties	15
8	Conclusion	16
	The ATLAS collaboration	19

1 Introduction

This paper summarizes the calibration procedure and reports the single-hit spatial resolution of the monitored drift tubes (MDT) in the ATLAS muon spectrometer (MS) during Run 2 of the Large Hadron Collider (LHC), spanning the 2015–2018 operating period. In this context, *single-hit* refers to the signal produced by a charged particle passing through a drift tube. The calibrations use data from both the spectrometer MDT chambers and a dedicated gas monitor MDT chamber (GMC), and are performed at the ATLAS muon calibration centers [1].

The MS design momentum resolution $\delta p/p$ is $\sim 3\%$ at 100 GeV and around 10% at 1 TeV [2], allowing both Standard Model measurements and new physics searches in processes containing high-momentum final-state muons [3]. Such searches may include the decay of heavy resonances into high transverse momentum (p_T) muons, demanding superior spectrometer performance for their discovery. For muons of p_T above 100 GeV, the drift tube single-hit resolution (and to a lesser extent, the chamber alignment) becomes an important contribution to the transverse momentum

resolution, and is the dominant factor above 250 GeV [2]. At high momentum, the p_T resolution σ_{p_T} is determined by the relation $\sigma_{p_T}/p_T \propto \sigma_{\text{res}} \times p_T$ [4], where σ_{res} is the single-hit spatial resolution. The design resolution is $\sigma_{\text{res}} = 80 \mu\text{m}$ [2].

The objective of the MDT calibration program is to achieve this resolution for all 354 000 drift tubes assembled into 1172 MDT chambers throughout all ATLAS data taking in LHC Run 2. The primary MDT calibration ingredients consist of tube t_0 timing offsets (referred to here as t_0 offsets or just t_0) and chamber-specific drift electron time to drift distance transfer relations, hereafter referred to as $R(t)$ functions. The t_0 offset is primarily a function of cable length and electronics delays, while the $R(t)$ function depends on the gas properties.

The operating conditions of the MDT detectors in the ATLAS cavern are characterized by large temperature gradients, occasional component faults, variations in humidity, background radiation, flow, pressure and mixture instabilities of the gas supply, all of which affect the timing response. In order to achieve the optimal resolution the calibration constants are routinely monitored, corrected for many of these second-order effects, and updated.

This paper describes the algorithms which generate a pair of correction parameters for the t_0 offsets and the $R(t)$ functions. These pairs of chamber-specific constants compensate for a number of systematic uncertainties associated with the operating conditions of the MDT chambers. As a final result, the MDT tube spatial resolution that has been achieved in ATLAS Run 2 is presented. Unless otherwise noted, all reported errors are statistical.

2 ATLAS detector

The ATLAS experiment [5] at the LHC is a multipurpose particle detector with a forward-backward symmetric cylindrical geometry and a near 4π coverage in solid angle.¹ It consists of an inner tracking detector (ID) surrounded by a thin superconducting solenoid providing a 2 T axial magnetic field, electromagnetic and hadronic calorimeters, and a muon spectrometer. The ID covers the pseudorapidity range $|\eta| < 2.5$. It consists of silicon pixel, silicon microstrip, and transition-radiation tracking detectors. Lead/liquid-argon (LAr) sampling calorimeters provide electromagnetic (EM) energy measurements with high granularity. A steel/scintillator-tile hadronic calorimeter covers the central pseudorapidity range ($|\eta| < 1.7$). The endcap and forward regions are instrumented with LAr calorimeters for EM and hadronic energy measurements up to $|\eta| = 4.9$.

The ATLAS muon spectrometer is cylindrical, 22 m in diameter and 45 m in length, surrounding the calorimeters with an acceptance coverage of 2π in azimuth and ± 2.7 in pseudorapidity. It consists of a barrel and two endcap sections located in an air-core toroidal magnetic field generated by eight coils for each section. The field integral of the toroids ranges between 2.0 and 6.0 T m for most of the acceptance, while the field magnitude at the MDT chambers ranges from near zero to 0.2 T in most of the endcap region ($1.05 < |\eta| < 2.7$), and averages about 0.6 T in the barrel ($|\eta| < 1.05$) region [2]. The MS identifies muons, provides muon triggers and, integrating with the

¹ATLAS uses a right-handed coordinate system with its origin at the nominal interaction point in the center of the detector and the z -axis along the beam pipe. The x -axis points from the interaction point to the center of the LHC ring, and the y -axis points upwards. Cylindrical coordinates (r, φ) are used in the transverse plane, φ being the azimuthal angle around the z -axis. The pseudorapidity is defined in terms of the polar angle θ as $\eta = -\ln \tan(\theta/2)$. The momentum in the transverse plane is denoted by p_T .

inner detector information, measures their charge sign and momenta. The MDT chambers perform precision charged-particle tracking in the plane defined by the beam axis (z) and the radial distance to the beam (r). The momentum measurement is based on the track curvature in these r - z coordinates, while resistive-plate chambers (RPC) and thin-gap chambers (TGC) provide triggering in the barrel and endcaps respectively, and readout of the so called *second coordinate* in the r - φ non-bending plane. The MDT chambers are assembled in three nested cylindrical barrel stations and three main coaxial discs in each of the endcap regions. A fourth annulus of endcap chambers covers a limited pseudorapidity region spanning from the barrel to the endcap. They are constructed of pairs of close-packed multilayers of 3 cm diameter cylindrical aluminum drift tubes, 1 m to 6 m long for the inner stations close to the beam and outer stations, respectively. Each multilayer comprises either three or four single planes, depending on the barrel (endcap) chamber radial (Z -axis) position, with each plane containing from 12 to 72 tubes. A 50 μm diameter anode wire is centered to within 30 μm of the axis of a 1.46 cm (1.5 cm) inner (outer) radius aluminum tube. The MDT gas is a mixture of 93% Ar and 7% CO_2 plus a few hundred ppm of water vapour at 3 bar pressure. The gas flows in a common trunk line to distribution racks and is fed in parallel to all drift tubes at a rate of roughly one tube volume per day. The total gas throughput to the entire MDT system is about 2×10^6 L/day. The tubes are operated at 3080 V anode voltage to deliver a gas avalanche amplification gain of 20 000. The single-hit efficiency for a minimum-ionizing particle is nearly 100% [6].

First-level triggers [7] are implemented in hardware and combine muon spectrometer and calorimeter measurements to accept events at a maximum rate of 100 kHz. These first-level triggers are followed by more refined software-based triggers that reduce the accepted event rate to 1 kHz on average.

3 Analysed data

The results presented here are based on a subset of the ATLAS Run 2 proton-proton collision data at a center-of-mass energy $\sqrt{s} = 13$ TeV. Specifically, this analysis uses 1.3 fb^{-1} of data that were acquired in 2015, 23.8 fb^{-1} in 2016, and 22.3 fb^{-1} in 2017. The 2015 and 2017 data include 7.9 pb^{-1} and 55.3 pb^{-1} , respectively, collected with the MS toroid magnet turned off. The data set is from the primary ATLAS physics data stream that includes all triggers and was processed with data quality selections common to all physics analyses. The selected set of data runs is distributed along the whole data acquisition period for each year, allowing checks of the stability of the parameters under study in different conditions. Each single run contains enough muon tracks per chamber to allow the determination of the $R(t)$ and resolution functions. Two corrections that depend on the non-bending plane second coordinate are applied to the time of the MDT signal by the offline event reconstruction software: (1) the magnetic-field-induced Lorentz angle effect on the drift time [8] and (2) the signal propagation time associated with the hit position along the wire.

This paper uses single-hit information from muon tracks with $p_{\text{T}} > 20$ GeV that are reconstructed in the ID and MS. The data include drift times, drift radii and timing offsets as used by the offline tracking reconstruction algorithms. A minimum of 1000 tube hits per chamber per run is required to obtain stable fit results in the analysis. As a consequence of these selection criteria the number of chambers for which results are obtained has a run-to-run variation of 0.3%. When

possible, multiple consecutive runs with the same gas conditions are grouped together in order to reach a minimum number of muon tracks per chamber.

4 MDT calibration

This section introduces the drift radius measurement and the basic calibration parameters necessary for its determination. The operational definition of the single-hit spatial resolution as applied in this analysis is then presented.

4.1 Drift radius determination

The MDT drift tube signal, or hit, provides the pulse arrival time, and a quantity reconstructed as the collected electric charge of the signal pulse. Read-out is accomplished with 24-channel front-end cards. These cards amplify, shape and discriminate the signals with programmable thresholds, then digitize the data. The hit time data are recorded in 1.2 μs windows initiated by a first-level trigger signal with a 0.78125 ns minimum digitization time. The charge contained in the leading edge of the signal is stored as voltage on a capacitor and read out as a run-down time using the Wilkinson technique [9].

The signal arrival time is relative to a specific proton-proton interaction time called the bunch crossing identifier. The bunch crossing time is measured in 25 ns ticks synchronized with an LHC global 40 MHz clock, and is subtracted in the read-out electronics hardware to yield the raw pulse arrival time. This pulse arrival time includes, in addition to the drift time, several timing offsets: the time-of-flight of the particle (muon) from the proton-proton interaction point to the tube, the signal propagation time along the tube wire, plus various fixed electronics and cable latencies. The sum of all these is referred to as the t_0 offset. The t_0 offset therefore represents the drift time produced by a particle crossing at the tube wire.

The raw time for every hit is converted into a drift time by subtracting the tube time offset. The drift time is a measure of the transit time of electrons generated by the primary ionization and subsequent avalanche multiplication to arrive at the anode wire. The resultant drift time is then mapped to the drift distance (circle) by means of a time-to-distance $R(t)$ transfer function, an example of which is shown in figure 1. The best straight line tangent to all such drift circles in a single chamber forms a track segment.

In ATLAS, the t_0 offset is a property of a single tube, whereas an $R(t)$ function is associated to a single MDT chamber. This association is valid to the extent that the operating conditions are uniform. Since chambers share a common high-voltage supply, gas pressure and thermal environment, these conditions are generally met at the chamber level. These t_0 offsets and $R(t)$ functions, globally called calibration constants, are generated by the ATLAS calibration computing centers.

4.2 t_0 determination

While the t_0 offset represents the drift time of a hit at the wire, operationally it is defined as the point of 50% of maximum amplitude of a Fermi-Dirac sigmoid function fit to the rising edge of an MDT drift time spectrum [10], as illustrated in figure 2. t_0 offsets are nominally determined for all tubes in the MS using single tube spectra or, when hit statistics are poor, the combined spectra from groups of 24 equal-length tubes sharing a common readout card. This t_0 offset definition is subject

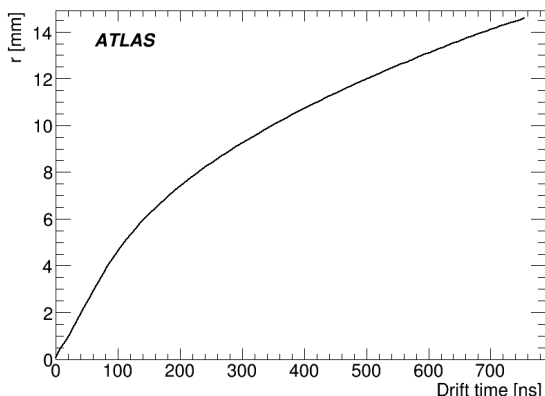


Figure 1. Gas monitor chamber $R(t)$ function for 93% Ar-7% CO_2 (and less than 0.1% of water vapour) for standard condition: 293 K, 3080 V and 3 bar, obtained via autocalibration.

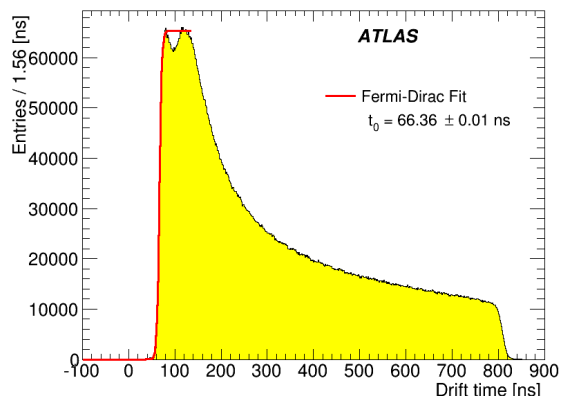


Figure 2. Measured drift time spectrum for a generic MDT chamber with a Fermi-Dirac function fit to the rising edge of the distribution.

to small systematic uncertainties of order 1 ns. These arise from different data selection, different background level and operating conditions in the GMC (see section 4.4) and the MDT systems, which affect the number of hits near the wire, the slope of the rising edge, and the subsequent fit result. These systematic effects are relevant for the GMC-based universal $R(t)$ function described in section 4.3 which is computed using the GMC t_0 offsets. They are resolved using a correction parameter, δt_0 , described in section 5.1.

4.3 $R(t)$ function determination

A standard method to extract the $R(t)$ function is by an autocalibration algorithm [11]. This algorithm, using a given set of t_0 offsets, iterates the linear fit to the drift radii in a chamber, each time updating the $R(t)$ function until the residuals converge to a minimum. An autocalibration $R(t)$ function is self-adapting to the chamber conditions, but a daily implementation of this procedure for every single MDT chamber requires significant computing resources and a large amount of data transfer and storage.

The alternative $R(t)$ function calibration method used here adopts the temperature-corrected universal $R(t)$ (URT), where the URT is the GMC $R(t)$ function derived using autocalibration for standard operating conditions (defined as gas pressure 3 bar, high voltage 3080 V, temperature 293 K, and GMC t_0 offsets). The URT method assumes that the absolute measured values of the chamber operating conditions of both the GMC and the MDT chambers are all known and that their differences can be corrected. The main sources of systematic differences resulting from this assumption are:

- The MDT chamber pressures can differ from the 3 bar nominal point due to several factors: local gas flow rates, pressure gauge location in the gas flow circuit, and pressure sensor offsets. Furthermore, sensors used in the GMC and in the MDT gas racks have systematic uncertainties of 10–20 mbar.
- The internal MDT gas temperature may be systematically misrepresented by the thermal sensors. There are typically eight sensors mounted on the tube walls at different locations in

the chamber. These sensors are read out periodically, and a daily average value over all sensors is computed. However, due to possible thermal gradients across the chambers (on average 1.8 ± 0.7 (RMS) K), and because the sensors are external to the tubes, this average temperature may not accurately represent the internal temperature everywhere in the gas volume.

- The actual high voltage supplied to chambers might deviate slightly (by about 1 V) from the nominal 3080 V operating voltage, although this has an effect of less than 0.1% on the maximum drift time. A larger high-voltage deviation generally indicates equipment failure, not a systematic error, and it is addressed during the detector access periods.

To correct for these effects a single catch-all parameter, referred to as effective pressure, δP , is defined. This parameter is used in a phenomenological correction function described in section 5.2.

In summary, an MDT chamber requires two types of calibrations: an $R(t)$ function and a set of t_0 offsets, each with a specific set of uncertainties. Two similar algorithms provide correction factors that compensate for these uncertainties and lead to improved single-hit spatial resolution.

4.4 Gas monitor chamber

The GMC [10] is an independent MDT chamber that operates in the surface gas facility, outside of the ATLAS experimental cavern. It has two gas partitions each independently sampling the common MDT trunk supply and exhaust lines that serve the entire MDT system, and records cosmic-ray muons at a rate of about 14 Hz. It is housed in a stable thermal enclosure where all operating parameters, gas flow, pressure, temperature, and high voltage, are continuously monitored.

The principal GMC output is a measurement of the maximum drift time, $t_{\max} = t_w - t_0$, where t_w is the arrival time of a hit located at the tube wall. A drift time spectrum, similar to figure 2, is computed for standard operating conditions by applying a correction function [12] based on the output of chamber-mounted pressure and temperature sensors. The tail end of the spectrum is fitted using a modified Fermi-Dirac sigmoid function similar to that used to obtain the t_0 offsets, and the t_{\max} is defined as a fit parameter, as described in ref. [10]. The t_{\max} is published hourly to the online run monitoring system and to the muon calibration centers. A variation of $t_{\max} > 1$ ns triggers the calculation of a new set of $R(t)$ functions for the track reconstruction. The t_{\max} is sensitive to small changes in the gas composition: for example, a 100 ppm absolute increase in water vapour content yields a nearly 7 ns increase in t_{\max} [13]. A single 24-hour period of GMC t_{\max} data is shown in figure 3, where the stability is better than 1 ns RMS. The GMC t_{\max} superimposed with the same quantity determined from the average of all chambers over the 2016 data-taking period is presented in figure 4. A one-time offset of -12 ns is applied to compensate for the typical difference in gas temperature between the MDT and the standard URT that range from about 4.5 to 5 K. The range of t_{\max} variation over one year is 15 ns. This change, observed annually, is attributed to the seasonal variation in ambient humidity in the ATLAS cavern that modulates the content of water vapour in the gas mixture.

The GMC produces URT functions every two hours. After local GMC temperature and pressure corrections are applied, the URT registers only changes in the gas composition. Based on the daily average of measurements from detector-mounted thermal sensors, the URT is converted into chamber-specific $R(t)$ functions [12]. These chamber $R(t)$ functions are further tuned by the δP correction parameter, as detailed in section 5.2.

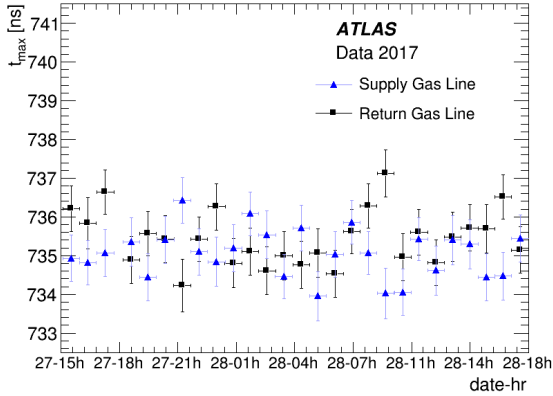


Figure 3. Hourly GMC measurements of t_{\max} over a single day during Run 2.

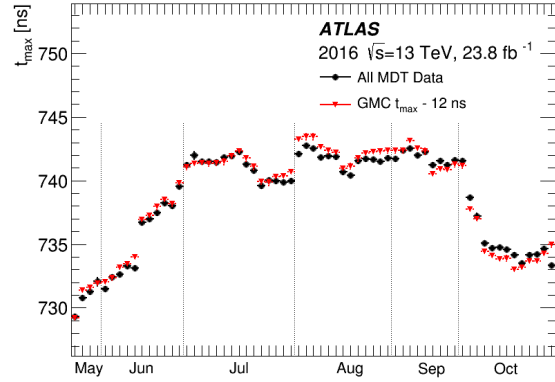


Figure 4. Measurement of t_{\max} daily average over the entire 2016 data-taking period, obtained from an average of all chambers and from the GMC. The horizontal axis represents run numbers, which are not uniformly distributed in time. Dotted lines delineate months.

4.5 Residuals and resolution

Track segments in a chamber are the best-fit straight lines tangent to the N circles defined by N drift radii. The distance of closest approach of a hit radius to this fit line is either a *fit* or *hit* residual. The former results when all N data points are included in the linear fit, and the latter is a measure of the j^{th} residual when the j^{th} point is excluded from the fit of the other $N - 1$ points. Hit and fit residual distributions (N entries per track, for all tracks in the analysed data set) are generated for each MDT chamber. Residuals are calculated for each of 15 radial bins, 1 mm wide, from 0 to 15 mm in drift radius r , as well as for a single 15-mm-wide radial bin. The former are used to obtain the radial dependence of the resolution and the latter is used to obtain the single-hit spatial resolution, both averaged over all tubes in a chamber. The residual distributions are fitted using a double-Gaussian function as expressed in equation (4.1): this choice is dictated by the stochastic nature of the signal formation that arises from ion-pair creation, gas diffusion and electron-ion transport and, importantly, allows for the dependence of the drift velocity on drift radius, as indicated by the non-linearity of the $R(t)$ function in figure 1. These properties produce residual distributions with radially dependent widths, including tails that are attributed to misassociated track hits from delta-rays and asynchronous background hits. While a single-Gaussian function inadequately describes the distributions for all radial bins, the double-Gaussian function used here provides a good fit to the residuals with a minimal increase in the number of free parameters. The fit function is:

$$f(r) = A_n e^{-\frac{(r-\bar{r})^2}{2\sigma_n^2}} + A_w e^{-\frac{(r-\bar{r})^2}{2\sigma_w^2}}, \quad (4.1)$$

where A_n , A_w , σ_n , σ_w are the amplitudes and standard deviations of a narrow and a wide Gaussian component. The two terms in equation (4.1) are constrained to a common mean \bar{r} , and fit over a residual range of ± 0.5 mm, which contains more than 99% of hits (section 7). The σ parameters (for fit and hit residuals) are determined for the r^{th} radial bin of the amplitude-weighted standard

deviations of the double-Gaussian function by:

$$\sigma(r) = \frac{A_n(r)\sigma_n(r) + A_w(r)\sigma_w(r)}{A_n(r) + A_w(r)}. \quad (4.2)$$

where the dependence of the fit parameters on the drift radius is explicitly indicated. Fit and hit residual distributions for a representative chamber at a drift radius near the wire, where the resolution is broader than far away from the wire, are shown in figures 5 and 6, respectively. These distributions are fit with the function of equation (4.1). For comparison purposes a single-Gaussian fit within the FWHM of these distributions is also shown.

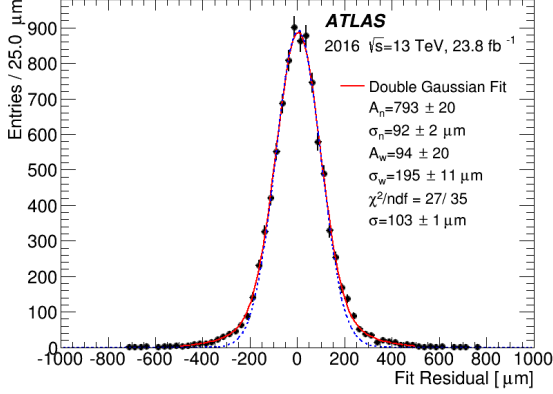


Figure 5. Fit residual distribution for a representative chamber for the radial bin $r = [2, 3]$ mm. A double-Gaussian (solid line) is fit in the range ± 0.5 mm. A single-Gaussian (dotted line) is fit within the FWHM but shown out to ± 0.5 mm.

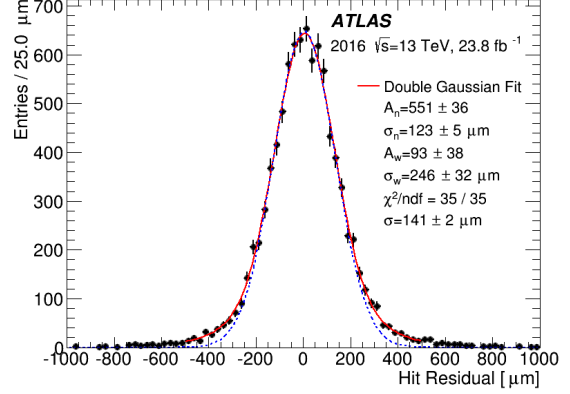


Figure 6. Hit residual distribution for the same chamber and radial bin as in figure 5.

The drift tube spatial resolution, σ_{res} , is the geometric mean of the fit and hit residual widths [14] defined as:

$$\sigma_{\text{res}}(r) = \sqrt{\sigma_{\text{fit}}(r) \cdot \sigma_{\text{hit}}(r)} \quad (4.3)$$

This approach was checked by Monte Carlo simulation. About 10^6 tracks incident on a generic chamber within a 10° angular range were generated. The drift radii assigned to these tracks were Gaussian distributed about their initial values using a radially dependent input resolution function derived from a test beam [15]. These smeared hit points were linearly fit and the output resolution for each radial bin was obtained using equation (4.3). The mean difference over the tube radius between the output and input resolution is $0.3 \pm 0.2 \mu\text{m}$, confirming the validity of the formulation.

5 Correction algorithms

This section describes the algorithms used to determine the δt_0 and δP corrections and their associated metrics, the track residuals and the resolution.

5.1 δt_0 correction

The default t_0 offset definition may vary by the order of 1 ns from the t_0 value that provides the best resolution. The algorithm described here is a variant of the tuning procedures designed to find the

best linear fit to a track segment by tuning the t_0 on a track-by-track basis [16]. The δt_0 correction method instead optimizes the default t_0 by testing a new, modified t_0 associated with a single chamber simultaneously for all tubes and for all tracks in a data run, while keeping the $R(t)$ function fixed. The algorithm operates on track segments containing at least as many hits as there are drift tube layers in the chamber, i.e. a minimum of six (eight) hits for a six-layer (eight-layer) chamber. The procedure steps through δt_0 over a range of ± 10 ns in 0.5 ns steps. At each step, new drift times and drift radii are computed and the segments are re-fit. Importantly, the residuals are evaluated only for hits with drift radii $r < 5$ mm where the drift velocity is largest, about $50 \mu\text{m}/\text{ns}$. By using only these near-wire residuals the procedure is practically insensitive to the $R(t)$ function and avoids compensating for systematic uncertainties which come into play at larger drift radii (see figure 12).

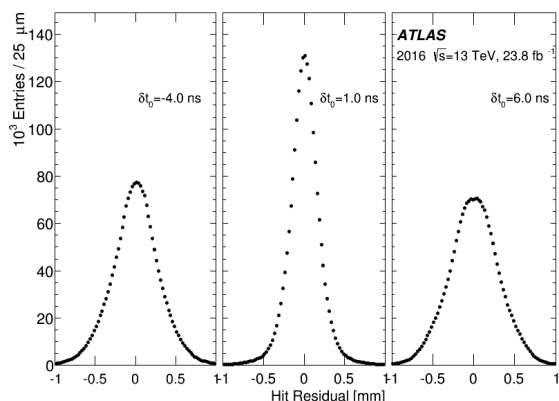


Figure 7. Hit residual distributions for a representative chamber for t_0 correction parameter set to -4 ns (left), $+1$ ns (center) and $+6$ ns (right) from the default value. Widths are 296, 188 and 303 μm , respectively.

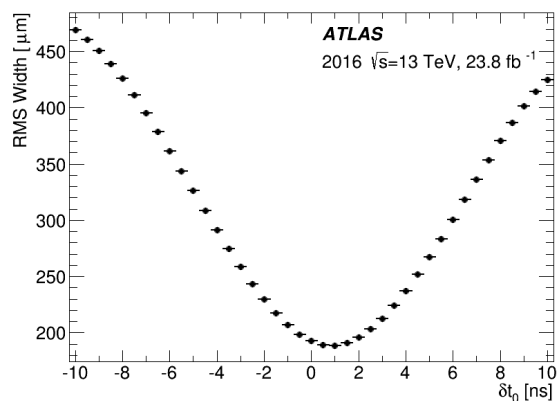


Figure 8. Typical RMS widths of hit residual distributions of hits less than 5 mm from the wire as a function of the t_0 correction, for the same chamber as in figure 7.

Figure 7 shows segment hit residuals from the t_0 correction procedure for a representative chamber for δt_0 values of -4 , $+1$, and $+6$ ns. Figure 8 shows the incremental change with each step of the residual RMS widths for the entire range of δt_0 values relative to the initial t_0 . The optimal δt_0 is the one yielding the minima of the RMS widths of the fit and hit residual distributions. The value on the vertical axis corresponding to the minimum in figure 8 does not represent the resolution, but only the RMS spread of the hit residuals near the wire.²

The δt_0 correction procedure is applied to 2015 data (the first year of Run 2 operation) using initial t_0 offsets generated by the MDT calibration centers. The δt_0 corrections obtained in a much higher peak-luminosity November 2015 run, $4.8 \times 10^{33} \text{ cm}^{-2} \text{ s}^{-1}$, are shown in figure 9, which reveals an average t_0 global correction of 1.3 ns with a RMS spread of 0.7 ns. The tails of the distribution are populated by a few chambers that were measured to have been constructed with structural non-conformities affecting the internal alignment of the tubes and therefore of the hit positions. The δt_0 correction tries to compensate for this misalignment.

²For over 95% of the MDT chambers the double-Gaussian fits yield the same t_0 minima as obtained using the RMS of the residual distributions. In the remaining chambers the fit method can lead to anomalous minima, so for consistency and stability of the results, the RMS method to establish the minimum is adopted for all chambers.

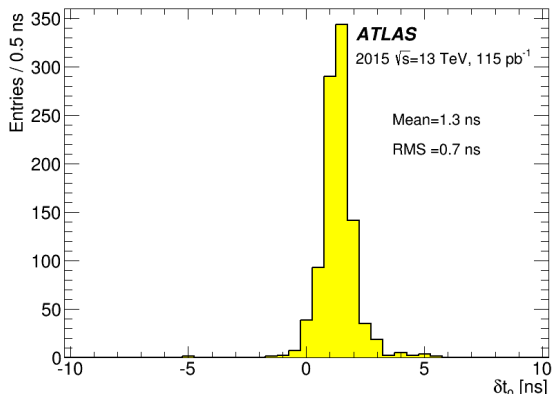


Figure 9. Distribution of δt_0 for one run in November 2015 determined by the t_0 correction algorithm.

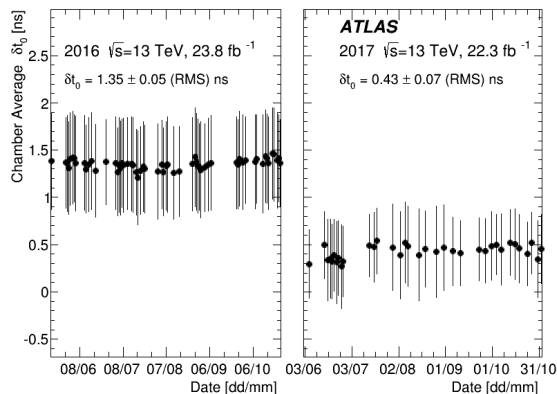


Figure 10. Chamber-averaged δt_0 values for runs in 2016 (left) and 2017 (right). Uncertainties are the RMS of the distributions.

The determination of the δt_0 corrections for all MDT chambers was repeated for a selection of data runs that span all data-taking periods in 2016 and 2017. The chamber-averaged δt_0 corrections for each run are shown in figure 10. At least 1165 out of the total 1172 chambers are included in each data point used for this average, depending on the integrated luminosity of the run. For the 65 runs analysed in 2016 the mean global δt_0 offset is 1.35 ± 0.05 (RMS) ns, consistent with the result determined from the 2015 data set. The δt_0 corrections from 2016 are then added to the calibration constants for 2017, so that the algorithm, when applied to the 2017 data set, produces a smaller global shift with a mean of 0.43 ± 0.07 (RMS) ns.

Figure 11 shows the chamber-by-chamber δt_0 difference between the first and last runs of the 2017 data set. In the first run, the toroid magnetic field was off and in the last run the field was at full strength and the instantaneous luminosity was higher by one order of magnitude. The mean difference is consistent with zero. This result demonstrates that the δt_0 parameter, once established, remains stable for all chambers over a large range of instantaneous luminosity and is insensitive to the magnetic field.

5.2 δP correction

Optimization of the $R(t)$ functions is done with an *effective pressure* parameter, δP , that corrects for the (small) inaccuracies in gas pressure sensors, temperature measurement, and high voltage. In all three cases, minor variations from nominal values produce radially dependent changes in the $R(t)$ function, such that a single, scalable correction function can be used. The calculation of this function is done using the Garfield program [17] configured to model the drift electron transport in MDT tubes with standard operating parameters as in section 2. Specifically, a pure Ar-CO₂ gas mixture without water vapour and zero magnetic field is used. Figure 12 shows the predicted change in the drift time as a function of drift radius for variations of temperature, pressure and high voltage from their reference values. This drift time response was previously validated with temperature data [12]. The maximum effect on the drift time is at the tube wall as expressed in equation (5.1), where the temperature correction is -2.6 ns/K, while the pressure correction function scales as -0.1 K/mbar relative to the temperature correction. The negative sign means that an increase in gas

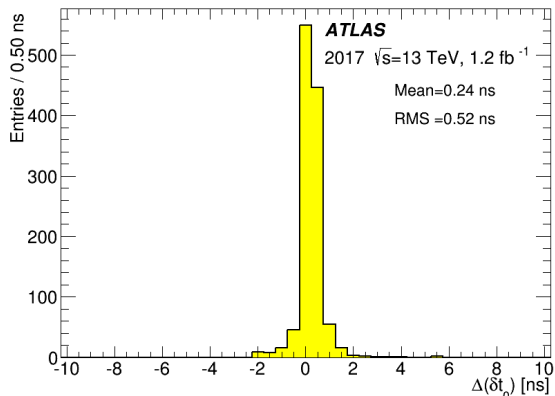


Figure 11. Chamber-by-chamber difference in the δt_0 parameter obtained from the June (toroid magnetic field off) and November (toroid magnetic field on) 2017 data.

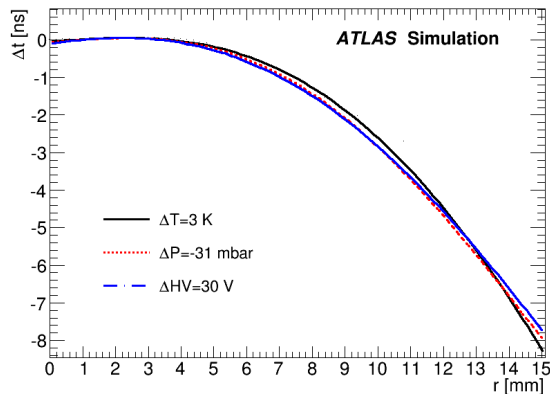


Figure 12. Garfield simulation of drift time variation as a function of drift radius for: +3 K, -31 mbar, and +30 V change relative to 293 K, 3 bar and 3080 V, respectively.

pressure at fixed temperature corresponds to an increase in gas density, a decreased drift electron mean free path, and thus longer drift times. Similarly, a higher voltage at fixed pressure leads to an increased electric field and higher drift velocity. Importantly, for any of these parameters, the curves in figure 12 indicate a negligible effect on drift times for radii smaller than 5 mm. For small deviations of the high voltage from the nominal setting, the drift time changes by only about 0.26 ns/V at the tube wall, thus typical systematic offsets of 1 V have a negligible effect:

$$\Delta t(\text{wall}) [\text{ns}] = -2.6 \frac{\text{ns}}{\text{K}} \times \Delta T [\text{K}] = +0.26 \frac{\text{ns}}{\text{mbar}} \times \Delta P [\text{mbar}] = -0.26 \frac{\text{ns}}{\text{V}} \times \Delta V [\text{V}]. \quad (5.1)$$

The effective pressure correction algorithm is similar to the δt_0 method and uses the same track-segment hit selection. For a collection of track-segment hits, δP is incremented in 5 mbar steps through a ± 100 mbar range of test pressures centered around the nominal 3 bar. The $R(t)$ function is recalculated using the correction function shown in figure 12 rescaled by the $P + \delta P$ effective pressure value assumed in the scan, new drift radii are obtained from the newly corrected $R(t)$ function, and track segments are re-fit and residuals evaluated. The procedure is initiated with the set of chamber-specific $R(t)$ functions of the day of the run. The δt_0 corrections found previously are applied to the hit drift times. For δP determination, the residuals are calculated for all drift radii.

Similar to the δt_0 procedure, the optimal δP is the one yielding the minimum of the RMS width of the fit and hit residual distributions. The hit residuals for three δP values, of -40 mbar, 10 mbar and 60 mbar, are shown for a representative chamber in figure 13. Figure 14 shows the RMS width of the hit residual distribution as a function of δP for the full scan range. The minimum at 10 mbar represents the best value of this parameter.

The minima of curves similar to figure 14, taken as the δP step corresponding to the lowest residual, were initially determined for all MDT chambers using data from August 2015 with the toroid magnet turned off. The algorithm was applied to a set of collision runs acquired 2.5 months later with the magnetic field turned on, and with 25 times higher instantaneous luminosity (from $0.17 \times 10^{33} \text{ cm}^{-2} \text{ s}^{-1}$ in mid August to $4.8 \times 10^{33} \text{ cm}^{-2} \text{ s}^{-1}$ at beginning of November), yielding in both cases an average correction δP of 30.0 ± 0.3 mbar with an 11 mbar RMS spread. Distributions

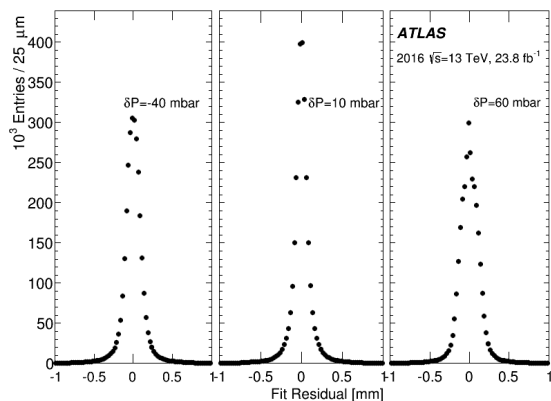


Figure 13. Fit residual distributions for a representative MDT chamber for $\delta P = -40$ mbar (left), $+10$ mbar (middle, optimal setting) and $+60$ mbar (right). RMS widths are 141, 131 and 144 μm , respectively.

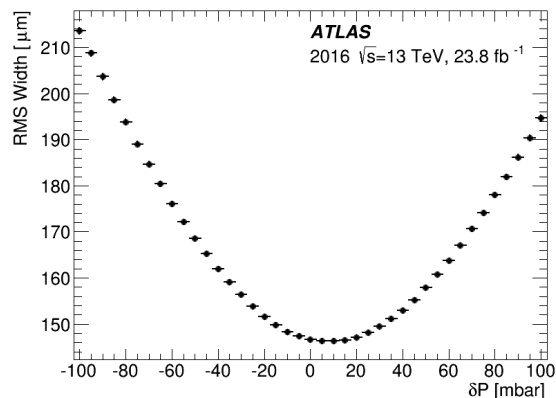


Figure 14. Fit residual RMS as a function of δP for the same chamber as in figure 13.

of the latter δP results are shown in figure 15, and the chamber-by-chamber differences in the δP correction for the two data sets are shown in figure 16. The measured change is within the δP step size. The corrections are stable in time and insensitive to both the magnetic field and the increased hit rates that result from higher instantaneous luminosity.

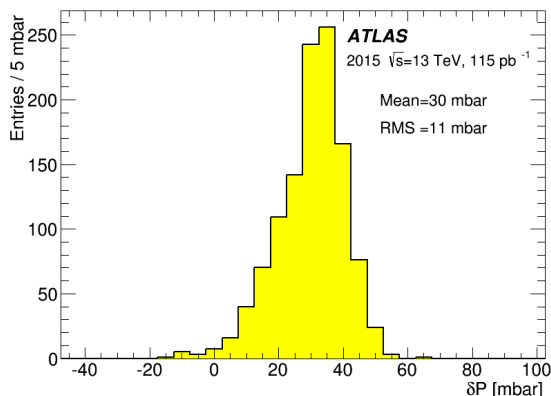


Figure 15. Distribution of δP for a high-luminosity run in November 2015.

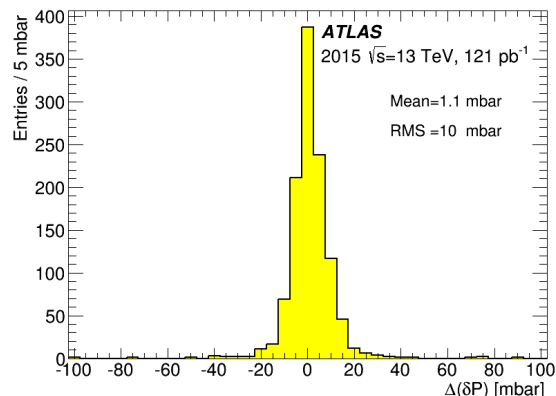


Figure 16. Chamber-by-chamber difference of δP for a run with the toroidal magnetic field off and a run 2.5 months later with 25 times higher luminosity and the toroid on.

The δP algorithm was further applied to 65 collision runs acquired from May to October 2016, where the peak luminosity exceeded $10^{34} \text{ cm}^{-2} \text{ s}^{-1}$, more than twice that of November 2015. These runs used $R(t)$ functions which included the δP corrections determined in the 2015 data. The chamber-averaged δP value for each of the runs in 2016 and 2017 is shown in figure 17 as a function of run date. The average of δP over all of 2016 data is 9.5 ± 0.8 mbar (RMS = 1.3 mbar) and for 2017 is 12.3 ± 1.0 mbar (RMS = 1.3 mbar). The δP correction is stable over each year to better than 3 mbar. Figure 18 shows the distribution of the chamber-by-chamber δP difference

between the first and last runs in the 2016 data set. The mean difference is 2.3 ± 4.5 (RMS) mbar, within the systematic uncertainty of the algorithm (section 7). This overall result supports the initial hypothesis that δP represents primarily systematic offsets of pressure gauges and other sensors and, once determined, would remain stable throughout a year of running.

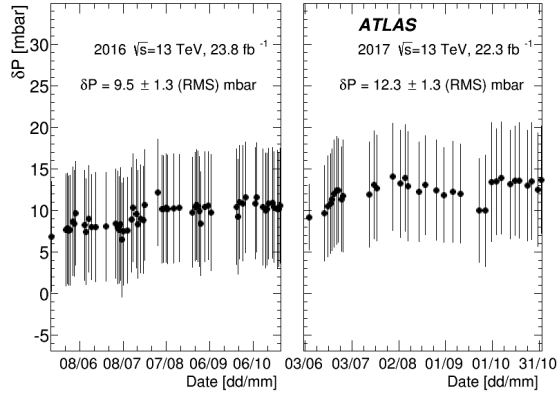


Figure 17. Chamber-averaged δP for each analysed run in 2016 (left) and 2017 (right). The uncertainties are the RMS spread of the chamber’s δP distribution.

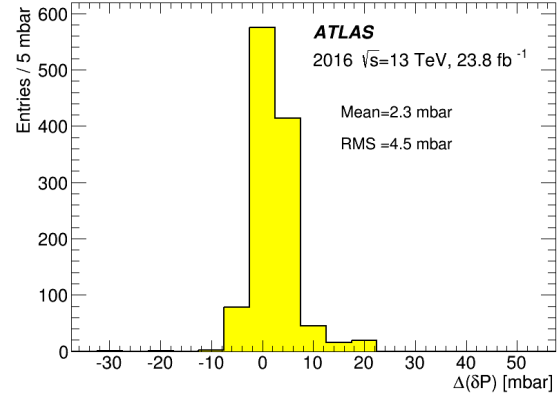


Figure 18. Chamber-by-chamber differences in δP between the first and last 2016 analysed run.

6 Resolution results

The single-hit MDT tube spatial resolution, as defined in equation (4.3), is measured in runs with the toroidal magnetic field on. A requirement of $p_T > 20$ GeV for the muon transverse momentum measured with the ID is applied to reduce the track curvature such that track segments could be reliably fit with a linear function, even in the chambers in a high magnetic field. For these tracks the negligible effects of the curvature due to magnetic field are folded into the systematic uncertainty.

The resolution obtained for a series of runs in each year of Run 2 is reported in figure 19. The full circles are calculated directly from fits to the default reconstructed track segments using the standard t_0 and $R(t)$ calibration constants. The triangles include the δt_0 corrections, and the blue inverted triangles also include δP corrections. Significant improvements to the resolution in 2015 are the result of a first implementation of the corrections, dominated by δP . These δP corrections were subsequently included in the standard production of $R(t)$ function calibration constants. The application of the procedure in each year yields 1–2 μm better resolution. The δt_0 corrections in 2015 and 2016 each lead to a 3–4 μm improvement in resolution. From the beginning of 2017 the previous year’s δt_0 corrections are also applied, but only the δP corrections from 2016 (not those from 2015). However, they yield an improvement of only 1.2 μm as shown in the right panel of figure 19.

Both the best δt_0 and δP values are incorporated in the end-of-year data reprocessing in order to provide the best calibrated data for subsequent physics analyses.

Figure 20 summarizes the resolution averaged over all runs in 2015, 2016, and 2017, for each MDT chamber. The left panels show the initial resolutions obtained with the standard calibrations. The right panels show the resolutions after all δt_0 and δP corrections are implemented and using

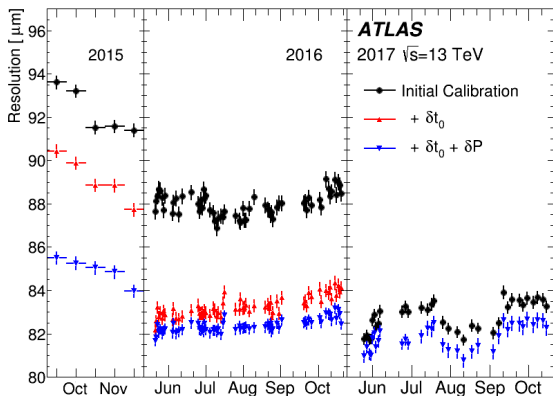


Figure 19. Resolution averaged over chambers for runs in 2015 (left), 2016 (center) and 2017 (right) using default calibrations, with δt_0 and δP corrections. The initial calibration data in the right panel already include the δt_0 corrections from 2016; additional δt_0 correction is not needed.

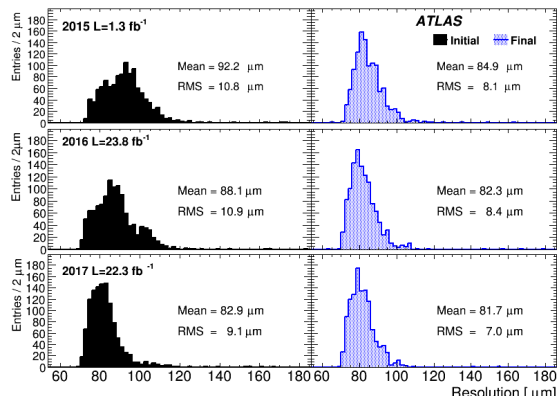


Figure 20. Single-hit resolutions for each chamber. Left: with default calibrations (different conditions every year). Right: with all corrections and most up-to-date $R(t)$ functions.

daily updated $R(t)$ functions: $84.9 \pm 0.2 \mu\text{m}$ for 2015, $82.3 \pm 0.2 \mu\text{m}$ for 2016, and $81.7 \pm 0.2 \mu\text{m}$ for 2017. Notably the improvements are measured both by the decrease of the mean value of the distribution and by the decrease of the RMS width, indicating greater uniformity of the resolutions of the whole ensemble of MDT chambers. In 2015, the δP corrections were applied for the first time in Run 2, and then incorporated into the default calibrations for 2016. In 2016, the larger data set allowed a much higher fraction of the initial t_0 offsets to be determined for single tubes by the calibration centers, resulting in a better overall initial resolution. The δt_0 corrections from 2016 were propagated into the default calibrations for 2017. For this reason, the incremental improvement in both the mean and the RMS spread decreases with each year and the standard offline tube resolution approaches the fully corrected result.

The final MDT drift tube spatial resolution, with all corrections described in previous sections included, is shown as a function of drift radius in figure 21 and in figure 22. In particular, figure 21 shows for 2016 the run-averaged resolution distributions $\sigma_{\text{res}}(r)$ in 1 mm radial bins, where each histogram bin entry represents a single chamber. This set of histograms therefore represents the full range of resolution functions obtained for the entire ensemble of MDT chambers. The mean values of these distributions are plotted as a single resolution function in figure 22, where the uncertainties are the RMS widths of the distributions for all chambers. For comparison, the resolution curves of a single MDT chamber deployed in a test beam [15], with and without background irradiation, are also displayed. The 2016 chamber-weighted resolution averaged over all radial bins is $86.4 \pm 0.2 \mu\text{m}$ and the average excluding the radial bin closest to the wire is $79.7 \pm 0.2 \mu\text{m}$. These two values bracket the final 2016 resolution averaged over all chambers, presented in figure 20, of $82.3 \pm 0.2 \mu\text{m}$.

Specific high instantaneous luminosity collision runs are analysed in order to measure the drift tube rates by counting all chamber hits occurring within the MDT read-out time window of $1.2 \mu\text{s}$ initiated by any muon trigger. This total number of hits per time window is normalized to the total tube area to obtain a rate per unit area. These rates are consistently less than 10 Hz/cm^2 ,

except for one set of 16 endcap inner chambers at high pseudorapidity whose rates range from 20 to 50 Hz/cm², and another set of 16 chambers nearest the beam-line where rates range from 60 to 140 Hz/cm². At background rates above 100 Hz/cm², some loss in tracking efficiency and resolution is expected due to increased read-out electronics dead time and space charge in the gas, respectively. Furthermore, an increase of the read-out electronics dead time was observed in special high instantaneous luminosity runs at the end of Run 1, and addressed in Run 2 by optimizing the data acquisition parameters. The resolutions from the analysed runs recorded in 2017 are entirely consistent with the results from 2016 shown here.

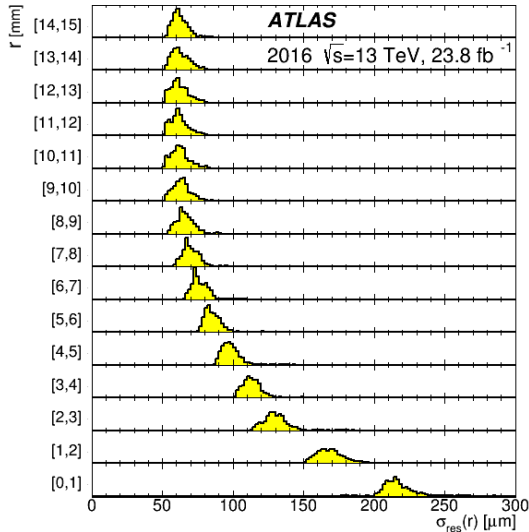


Figure 21. Distribution of resolutions in 1 mm radial bins of drift radius for all MDT chambers, averaged over all analysed runs from 2016.

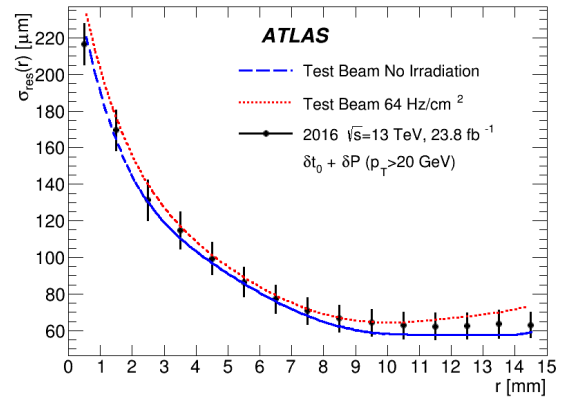


Figure 22. Resolution as a function of drift radius averaged over all MDT chambers and all analysed runs from 2016. Muon test-beam resolutions of an MDT chamber with background radiation from 0 to 64 Hz/cm² are also shown for comparison [15]. Uncertainties are RMS widths of the resolution distribution for all chambers.

7 Systematic uncertainties

The main sources of systematic uncertainty affecting the determination of the MDT resolution are: (1) the fit uncertainty associated with the range of the double-Gaussian fit; (2) the use of linear fits for curved track segments; (3) the precision of the δt_0 and δP determinations; and (4) the accuracy of equation (4.3) to describe the resolution. They are described in this section.

A double-Gaussian function is fit in a range of ± 500 μm for both the fit and hit residual distributions. This fit function matches well the central region with a narrow component and the tails with the wider component. The fraction of hits included in the residual distributions exceeds 99% for most drift radii, and (95–97)% for the first millimeter nearest the wire. The reason for this additional loss is attributed to the minimum 1 mm path length corresponding to the MDT front-end electronics threshold of 23 primary ionization electrons [9]. For radial distances below 1 mm,

the precision of the drift radius determination deteriorates due to the small number of ion pairs, increasing the fraction of large residuals. A modification of the fit range down to $\pm 400 \mu\text{m}$ and up to $\pm 1 \text{ mm}$ produces an overall systematic variation in the resolution of $1 \mu\text{m}$.

The path of a low- p_{T} muon track is slightly deflected by the magnetic field as it passes through a chamber. For this reason, the tracks used in the analysis have a minimum transverse momentum of 20 GeV , yielding an average p_{T} of 40 GeV . The systematic resolution broadening from using a linear fit is determined from a Monte Carlo calculation using a worst-case 0.6 T magnetic field and for the most prevalent MDT geometry: a six-layer chamber with a 17 cm spacer frame separating the two multilayers. The hits are smeared with the nominal $80 \mu\text{m}$ resolution, linearly fit to generate residuals, and the resolution computed from equation (4.3). The average resolution for $p_{\text{T}} = 40 \text{ GeV}$ muons is broadened by about $2 \mu\text{m}$ relative to the nominal value. In addition, this uncertainty from track curvature in the magnetic field is also directly investigated by comparing the resolutions obtained with and without the toroidal magnetic field. The average resolution of all chambers with the toroid field off is $\sigma_{\text{off}} = 80.1 \pm 0.2 \mu\text{m}$. The average broadening of the measured resolution due to the toroidal field is $1.6 \pm 0.3 \mu\text{m}$, consistent with the result from Monte Carlo calculation.

The step of the correction algorithm is 0.5 ns for δt_0 and 5 mbar for δP . The minima are found separately for the hit and fit residual distributions, and agree to within one step for more than 90% of the chambers. Therefore, the precision with which the parameters can be reliably established is estimated to be half of the step size. The uncertainty for each parameter is determined by altering the optimal δt_0 and δP values within $\pm 0.25 \text{ ns}$ for δt_0 and $\pm 2.5 \text{ mbar}$ for δP and recalculating the resolution functions. The average systematic uncertainty in the correction parameter determination is $1 \mu\text{m}$.

A final, small systematic uncertainty derives from the accuracy to which the resolution function of equation (4.2) reproduces the true resolution. This uncertainty, described in section 4.5, is $0.3 \mu\text{m}$.

The total systematic error of the single-hit spatial resolution measurement, taken as the sum in quadrature of all contributions, is $2.2 \mu\text{m}$, as summarized in table 1, and about 2.6% of the overall average resolution.

Table 1. Main resolution systematic uncertainties averaged over all chambers.

Systematic uncertainty	Size [μm]
Double-Gaussian fit range	1.0
Straight-line track fit	1.6
Optimal δP and δt_0 values	1.0
Resolution function accuracy	0.3
Total	2.2

8 Conclusion

This document describes a novel method to optimize the single-hit spatial resolution of the muon MDT chambers of the ATLAS experiment during Run 2 of the LHC. This method tunes the initial t_0 derived from drift time spectra and provides a correction parameter for $R(t)$ functions produced

by a gas monitor MDT chamber. The extracted corrections were used in the 2015 and 2016 end-of-year data reprocessing, and became fully integrated in the online calibrations from 2017 onward, yielding results consistent with those presented here. These two combined correction parameters are shown to be very stable over a year, insensitive to increasing luminosity, variations in environmental conditions, or the magnetic field. The method applied to the 2017 data achieves a mean single-hit spatial resolution of $81.7 \pm 0.2 \pm 2.2$ (sys) μm with an RMS spread of $7 \mu\text{m}$ over all 1172 MDT chambers in the spectrometer. The resolution approaches the design value of $80 \mu\text{m}$, consistent over all MDT chambers, and stable across all run periods.

Acknowledgments

We thank CERN for the very successful operation of the LHC, as well as the support staff from our institutions without whom ATLAS could not be operated efficiently.

We acknowledge the support of ANPCyT, Argentina; YerPhI, Armenia; ARC, Australia; BMWFW and FWF, Austria; ANAS, Azerbaijan; SSTC, Belarus; CNPq and FAPESP, Brazil; NSERC, NRC and CFI, Canada; CERN; CONICYT, Chile; CAS, MOST and NSFC, China; COLCIENCIAS, Colombia; MSMT CR, MPO CR and VSC CR, Czech Republic; DNRF and DNSRC, Denmark; IN2P3-CNRS, CEA-DRF/IRFU, France; SRNSFG, Georgia; BMBF, HGF, and MPG, Germany; GSRT, Greece; RGC, Hong Kong SAR, China; ISF and Benozziyo Center, Israel; INFN, Italy; MEXT and JSPS, Japan; CNRST, Morocco; NWO, Netherlands; RCN, Norway; MNiSW and NCN, Poland; FCT, Portugal; MNE/IFA, Romania; MES of Russia and NRC KI, Russian Federation; JINR; MESTD, Serbia; MSSR, Slovakia; ARRS and MIZŠ, Slovenia; DST/NRF, South Africa; MINECO, Spain; SRC and Wallenberg Foundation, Sweden; SERI, SNSF and Cantons of Bern and Geneva, Switzerland; MOST, Taiwan; TAEK, Turkey; STFC, United Kingdom; DOE and NSF, United States of America. In addition, individual groups and members have received support from BCKDF, CANARIE, CRC and Compute Canada, Canada; COST, ERC, ERDF, Horizon 2020, and Marie Skłodowska-Curie Actions, European Union; Investissements d’Avenir Labex and Idex, ANR, France; DFG and AvH Foundation, Germany; Herakleitos, Thales and Aristeia programmes co-financed by EU-ESF and the Greek NSRF, Greece; BSF-NSF and GIF, Israel; CERCA Programme Generalitat de Catalunya, Spain; The Royal Society and Leverhulme Trust, United Kingdom.

The crucial computing support from all WLCG partners is acknowledged gratefully, in particular from CERN, the ATLAS Tier-1 facilities at TRIUMF (Canada), NDGF (Denmark, Norway, Sweden), CC-IN2P3 (France), KIT/GridKA (Germany), INFN-CNAF (Italy), NL-T1 (Netherlands), PIC (Spain), ASGC (Taiwan), RAL (U.K.) and BNL (U.S.A.), the Tier-2 facilities worldwide and large non-WLCG resource providers. Major contributors of computing resources are listed in ref. [18].

References

- [1] T. Dai et al., *The ATLAS MDT remote calibration centers*, *J. Phys. Conf. Ser.* **219** (2010) 022028.
- [2] ATLAS collaboration, *ATLAS muon spectrometer: technical design report*, CERN-LHCC-97-022, CERN, Geneva, Switzerland (1997).

- [3] ATLAS collaboration, *Search for new high-mass phenomena in the dilepton final state using 36fb^{-1} of proton-proton collision data at $\sqrt{s} = 13\text{ TeV}$ with the ATLAS detector*, *JHEP* **10** (2017) 182 [[arXiv:1707.02424](#)].
- [4] ATLAS collaboration, *Muon reconstruction efficiency and momentum resolution of the ATLAS experiment in proton-proton collisions at $\sqrt{s} = 7\text{ TeV}$ in 2010*, *Eur. Phys. J. C* **74** (2014) 3034 [[arXiv:1404.4562](#)].
- [5] ATLAS collaboration, *The ATLAS experiment at the CERN Large Hadron Collider*, 2008 *JINST* **3** S08003.
- [6] ATLAS collaboration, *Commissioning of the ATLAS muon spectrometer with cosmic rays*, *Eur. Phys. J. C* **70** (2010) 875 [[arXiv:1006.4384](#)].
- [7] ATLAS collaboration, *Performance of the ATLAS trigger system in 2015*, *Eur. Phys. J. C* **77** (2017) 317 [[arXiv:1611.09661](#)].
- [8] S. Horvat et al., *Operation of the ATLAS muon drift-tube chambers at high background rates and in magnetic fields*, *IEEE Trans. Nucl. Sci.* **53** (2006) 562.
- [9] Y. Arai et al., *ATLAS muon drift tube electronics*, 2008 *JINST* **3** P09001.
- [10] D.S. Levin et al., *Drift time spectrum and gas monitoring in the ATLAS muon spectrometer precision chambers*, *Nucl. Instrum. Meth. A* **588** (2008) 347.
- [11] C. Bacci et al., *Autocalibration of high precision drift tubes*, *Nucl. Phys. Proc. Suppl. B* **54** (1997) 311.
- [12] N. Amram et al., *Streamlined calibrations of the ATLAS precision muon chambers for initial LHC running*, *Nucl. Instrum. Meth. A* **671** (2012) 40 [[arXiv:1103.0797](#)].
- [13] N. Amram et al., *Gas performance of the ATLAS MDT precision chambers*, *IEEE Nucl. Sci. Symp. Conf. Rec.* (2008) 3213.
- [14] R.K. Carnegie et al., *Resolution studies of cosmic ray tracks in a TPC with GEM readout*, *Nucl. Instrum. Meth. A* **538** (2005) 372 [[physics/0402054](#)].
- [15] M. Deile et al., *Performance of the ATLAS precision muon chambers under LHC operating conditions*, *Nucl. Instrum. Meth. A* **518** (2004) 65 [[arXiv:1604.00236](#)].
- [16] P. Branchini, F. Ceradini, S.D. Luise, M. Iodice and F. Petrucci, *Global time fit for tracking in an array of drift cells: the drift tubes of the ATLAS experiment*, *IEEE Trans. Nucl. Sci.* **55** (2008) 620.
- [17] R. Veenhof, *Garfield, a drift-chamber simulation program*, CERN program library entry W5050, CERN, Geneva, Switzerland (1993).
- [18] ATLAS collaboration, *ATLAS computing acknowledgements*, *ATL-GEN-PUB-2016-002*, CERN, Geneva, Switzerland (2016).

The ATLAS collaboration

G. Aad¹⁰¹, B. Abbott¹²⁸, D.C. Abbott¹⁰², O. Abidin^{13,*}, A. Abed Abud^{70a,70b}, K. Abeling⁵³, D.K. Abhayasinghe⁹³, S.H. Abidi¹⁶⁷, O.S. AbouZeid⁴⁰, N.L. Abraham¹⁵⁶, H. Abramowicz¹⁶¹, H. Abreu¹⁶⁰, Y. Abulaiti⁶, B.S. Acharya^{66a,66b,n}, B. Achkar⁵³, S. Adachi¹⁶³, L. Adam⁹⁹, C. Adam Bourdarios¹³², L. Adamczyk^{83a}, L. Adamek¹⁶⁷, J. Adelman¹²¹, M. Adersberger¹¹⁴, A. Adiguzel^{12c,ai}, S. Adorni⁵⁴, T. Adye¹⁴⁴, A.A. Affolder¹⁴⁶, Y. Afik¹⁶⁰, C. Agapopoulou¹³², M.N. Agaras³⁸, A. Aggarwal¹¹⁹, C. Agheorghiesei^{27c}, J.A. Aguilar-Saavedra^{140f,140a,ah}, F. Ahmadov⁷⁹, W.S. Ahmed¹⁰³, X. Ai¹⁸, G. Aielli^{73a,73b}, S. Akatsuka⁸⁵, T.P.A. Åkesson⁹⁶, E. Akilli⁵⁴, A.V. Akimov¹¹⁰, K. Al Khoury¹³², G.L. Alberghi^{23b,23a}, J. Albert¹⁷⁶, M.J. Alconada Verzini⁸⁸, S. Alderweireldt³⁶, M. Aleksa³⁶, I.N. Aleksandrov⁷⁹, C. Alexa^{27b}, D. Alexandre¹⁹, T. Alexopoulos¹⁰, A. Alfonsi¹²⁰, M. Alhroob¹²⁸, B. Ali¹⁴², G. Alimonti^{68a}, J. Alison³⁷, S.P. Alkire¹⁴⁸, C. Allaire¹³², B.M.M. Allbrooke¹⁵⁶, B.W. Allen¹³¹, P.P. Allport²¹, A. Aloisio^{69a,69b}, A. Alonso⁴⁰, F. Alonso⁸⁸, C. Alpigiani¹⁴⁸, A.A. Alshehri⁵⁷, M. Alvarez Estevez⁹⁸, D. Álvarez Piqueras¹⁷⁴, M.G. Alviggi^{69a,69b}, Y. Amaral Coutinho^{80b}, A. Ambler¹⁰³, L. Ambroz¹³⁵, C. Amelung²⁶, D. Amidei¹⁰⁵, S.P. Amor Dos Santos^{140a}, S. Amoroso⁴⁶, C.S. Amrouche⁵⁴, F. An⁷⁸, C. Anastopoulos¹⁴⁹, N. Andari¹⁴⁵, T. Andeen¹¹, C.F. Anders^{61b}, J.K. Anders²⁰, A. Andreazza^{68a,68b}, V. Andrei^{61a}, C.R. Anelli¹⁷⁶, S. Angelidakis³⁸, A. Angerami³⁹, A.V. Anisenkov^{122b,122a}, A. Annovi^{71a}, C. Antel^{61a}, M.T. Anthony¹⁴⁹, M. Antonelli⁵¹, D.J.A. Antrim¹⁷¹, F. Anulli^{72a}, M. Aoki⁸¹, J.A. Aparisi Pozo¹⁷⁴, L. Aperio Bella³⁶, G. Arabidze¹⁰⁶, J.P. Araque^{140a}, V. Araujo Ferraz^{80b}, R. Araujo Pereira^{80b}, C. Arcangeletti⁵¹, A.T.H. Arce⁴⁹, F.A. Arduh⁸⁸, J-F. Arguin¹⁰⁹, S. Argyropoulos⁷⁷, J.-H. Arling⁴⁶, A.J. Armbruster³⁶, A. Armstrong¹⁷¹, O. Arnaez¹⁶⁷, H. Arnold¹²⁰, A. Artamonov^{111,*}, G. Artoni¹³⁵, S. Artz⁹⁹, S. Asai¹⁶³, N. Asbah⁵⁹, E.M. Asimakopoulou¹⁷², L. Asquith¹⁵⁶, K. Assamagan²⁹, R. Astalos^{28a}, R.J. Atkin^{33a}, M. Atkinson¹⁷³, N.B. Atlay¹⁵¹, H. Atmani¹³², K. Augsten¹⁴², G. Avolio³⁶, R. Avramidou^{60a}, M.K. Ayoub^{15a}, A.M. Azoulay^{168b}, G. Azuelos^{109,ax}, M.J. Baca²¹, H. Bachacou¹⁴⁵, K. Bachas^{67a,67b}, M. Backes¹³⁵, F. Backman^{45a,45b}, P. Bagnaia^{72a,72b}, M. Bahmani⁸⁴, H. Bahrasemani¹⁵², A.J. Bailey¹⁷⁴, V.R. Bailey¹⁷³, J.T. Baines¹⁴⁴, M. Bajic⁴⁰, C. Bakalis¹⁰, O.K. Baker¹⁸³, P.J. Bakker¹²⁰, D. Bakshi Gupta⁸, S. Balaji¹⁵⁷, E.M. Baldin^{122b,122a}, P. Balek¹⁸⁰, F. Balli¹⁴⁵, W.K. Balunas¹³⁵, J. Balz⁹⁹, E. Banas⁸⁴, A. Bandyopadhyay²⁴, Sw. Banerjee^{181,i}, A.A.E. Bannoura¹⁸², L. Barak¹⁶¹, W.M. Barbe³⁸, E.L. Barberio¹⁰⁴, D. Barberis^{55b,55a}, M. Barbero¹⁰¹, T. Barillari¹¹⁵, M.-S. Barisits³⁶, J. Barkeloo¹³¹, T. Barklow¹⁵³, R. Barnea¹⁶⁰, S.L. Barnes^{60c}, B.M. Barnett¹⁴⁴, R.M. Barnett¹⁸, Z. Barnovska-Blenessy^{60a}, A. Baroncelli^{60a}, G. Barone²⁹, A.J. Barr¹³⁵, L. Barranco Navarro^{45a,45b}, F. Barreiro⁹⁸, J. Barreiro Guimarães da Costa^{15a}, S. Barsov¹³⁸, R. Bartoldus¹⁵³, G. Bartolini¹⁰¹, A.E. Barton⁸⁹, P. Bartos^{28a}, A. Basalae⁴⁶, A. Bassalat^{132,aq}, R.L. Bates⁵⁷, S.J. Batista¹⁶⁷, S. Batlamous^{35e}, J.R. Batley³², B. Batool¹⁵¹, M. Battaglia¹⁴⁶, M. Bauge^{72a,72b}, F. Bauer¹⁴⁵, K.T. Bauer¹⁷¹, H.S. Bawa^{31,1}, J.B. Beacham⁴⁹, T. Beau¹³⁶, P.H. Beauchemin¹⁷⁰, F. Becherer⁵², P. Bechtel²⁴, H.C. Beck⁵³, H.P. Beck^{20,r}, K. Becker⁵², M. Becker⁹⁹, C. Becot⁴⁶, A. Beddall^{12d}, A.J. Beddall^{12a}, V.A. Bednyakov⁷⁹, M. Bedognetti¹²⁰, C.P. Bee¹⁵⁵, T.A. Beermann⁷⁶, M. Begalli^{80b}, M. Begel²⁹, A. Behera¹⁵⁵, J.K. Behr⁴⁶, F. Beisiegel²⁴, A.S. Bell⁹⁴, G. Bella¹⁶¹, L. Bellagamba^{23b}, A. Bellerive³⁴, P. Bellos⁹, K. Beloborodov^{122b,122a}, K. Belotskiy¹¹², N.L. Belyaev¹¹², D. Benchebkroun^{35a}, N. Benekos¹⁰, Y. Benhammou¹⁶¹, D.P. Benjamin⁶, M. Benoit⁵⁴, J.R. Bensinger²⁶, S. Bentvelsen¹²⁰, L. Beresford¹³⁵, M. Beretta⁵¹, D. Berge⁴⁶, E. Bergeaas Kuutmann¹⁷², N. Berger⁵, B. Bergmann¹⁴², L.J. Bergsten²⁶, J. Beringer¹⁸, S. Berlendis⁷, N.R. Bernard¹⁰², G. Bernardi¹³⁶, C. Bernius¹⁵³, T. Berry⁹³, P. Berta⁹⁹, C. Bertella^{15a}, I.A. Bertram⁸⁹, G.J. Besjes⁴⁰, O. Bessidskaia Bylund¹⁸², N. Besson¹⁴⁵, A. Bethani¹⁰⁰, S. Bethke¹¹⁵, A. Betti²⁴, A.J. Bevan⁹², J. Beyer¹¹⁵, R. Bi¹³⁹, R.M. Bianchi¹³⁹, O. Biebel¹¹⁴, D. Biedermann¹⁹, R. Bielski³⁶, K. Bierwagen⁹⁹, N.V. Biesuz^{71a,71b}, M. Biglietti^{74a}, T.R.V. Billoud¹⁰⁹, M. Bindi⁵³, A. Bingul^{12d}, C. Bini^{72a,72b}, S. Biondi^{23b,23a}, M. Birman¹⁸⁰, T. Bisanz⁵³, J.P. Biswal¹⁶¹, A. Bitadze¹⁰⁰, C. Bittrich⁴⁸, K. Björke¹³⁴, K.M. Black²⁵, T. Blazek^{28a}, I. Bloch⁴⁶, C. Blocker²⁶, A. Blue⁵⁷, U. Blumenschein⁹², G.J. Bobbink¹²⁰, V.S. Bobrovnikov^{122b,122a}, S.S. Bocchetta⁹⁶, A. Bocci⁴⁹,

D. Boerner⁴⁶, D. Bogavac¹⁴, A.G. Bogdanchikov^{122b,122a}, C. Bohm^{45a}, V. Boisvert⁹³, P. Bokan^{53,172},
 T. Bold^{83a}, A.S. Boldyrev¹¹³, A.E. Bolz^{61b}, M. Bomben¹³⁶, M. Bona⁹², J.S. Bonilla¹³¹, M. Boonekamp¹⁴⁵,
 H.M. Borecka-Bielska⁹⁰, A. Borisov¹²³, G. Borissov⁸⁹, J. Bortfeldt³⁶, D. Bortoletto¹³⁵, V. Bortolotto^{73a,73b},
 D. Boscherini^{23b}, M. Bosman¹⁴, J.D. Bossio Sola¹⁰³, K. Bouaouda^{35a}, J. Boudreau¹³⁹,
 E.V. Bouhova-Thacker⁸⁹, D. Boumediene³⁸, S.K. Boutle⁵⁷, A. Boveia¹²⁶, J. Boyd³⁶, D. Boye^{33b,ar},
 I.R. Boyko⁷⁹, A.J. Bozson⁹³, J. Bracinek²¹, N. Brahimi¹⁰¹, G. Brandt¹⁸², O. Brandt^{61a}, F. Braren⁴⁶,
 B. Brau¹⁰², J.E. Brau¹³¹, W.D. Breaden Madden⁵⁷, K. Brendlinger⁴⁶, L. Brenner⁴⁶, R. Brenner¹⁷²,
 S. Bressler¹⁸⁰, B. Brickwedde⁹⁹, D.L. Briglin²¹, D. Britton⁵⁷, D. Britzger¹¹⁵, I. Brock²⁴, R. Brock¹⁰⁶,
 G. Brooijmans³⁹, W.K. Brooks^{147b}, E. Brost¹²¹, J.H. Broughton²¹, P.A. Bruckman de Renstrom⁸⁴,
 D. Bruncko^{28b}, A. Bruni^{23b}, G. Bruni^{23b}, L.S. Bruni¹²⁰, S. Bruno^{73a,73b}, B.H. Brunt³², M. Bruschi^{23b},
 N. Brusino¹³⁹, P. Bryant³⁷, L. Bryngemark⁹⁶, T. Buanes¹⁷, Q. Buat³⁶, P. Buchholz¹⁵¹, A.G. Buckley⁵⁷,
 I.A. Budagov⁷⁹, M.K. Bugge¹³⁴, F. Bühner⁵², O. Bulekov¹¹², T.J. Burch¹²¹, S. Burdin⁹⁰, C.D. Burgard¹²⁰,
 A.M. Burger¹²⁹, B. Burghgrave⁸, K. Burka⁸⁴, J.T.P. Burr⁴⁶, J.C. Burzynski¹⁰², V. Büscher⁹⁹,
 E. Buschmann⁵³, P.J. Bussey⁵⁷, J.M. Butler²⁵, C.M. Buttar⁵⁷, J.M. Butterworth⁹⁴, P. Butti³⁶,
 W. Buttinger³⁶, A. Buzatu¹⁵⁸, A.R. Buzykaev^{122b,122a}, G. Cabras^{23b,23a}, S. Cabrera Urbán¹⁷⁴, D. Caforio⁵⁶,
 H. Cai¹⁷³, V.M.M. Cairo¹⁵³, O. Cakir^{4a}, N. Calace³⁶, P. Calafiura¹⁸, A. Calandri¹⁰¹, G. Calderini¹³⁶,
 P. Calfayan⁶⁵, G. Callea⁵⁷, L.P. Caloba^{80b}, S. Calvente Lopez⁹⁸, D. Calvet³⁸, S. Calvet³⁸, T.P. Calvet¹⁵⁵,
 M. Calvetti^{71a,71b}, R. Camacho Toro¹³⁶, S. Camarda³⁶, D. Camarero Munoz⁹⁸, P. Camarri^{73a,73b},
 D. Cameron¹³⁴, R. Caminal Armadans¹⁰², C. Camincher³⁶, S. Campana³⁶, M. Campanelli⁹⁴,
 A. Camplani⁴⁰, A. Campoverde¹⁵¹, V. Canale^{69a,69b}, A. Canesse¹⁰³, M. Cano Bret^{60c}, J. Cantero¹²⁹,
 T. Cao¹⁶¹, Y. Cao¹⁷³, M.D.M. Capeans Garrido³⁶, M. Capua^{41b,41a}, R. Cardarelli^{73a}, F.C. Cardillo¹⁴⁹,
 G. Carducci^{41b,41a}, I. Carli¹⁴³, T. Carli³⁶, G. Carlino^{69a}, B.T. Carlson¹³⁹, L. Carminati^{68a,68b},
 R.M.D. Carney^{45a,45b}, S. Caron¹¹⁹, E. Carquin^{147b}, S. Carrá⁴⁶, J.W.S. Carter¹⁶⁷, M.P. Casado^{14,d},
 A.F. Casha¹⁶⁷, D.W. Casper¹⁷¹, R. Castelijin¹²⁰, F.L. Castillo¹⁷⁴, V. Castillo Gimenez¹⁷⁴,
 N.F. Castro^{140a,140e}, A. Catinaccio³⁶, J.R. Catmore¹³⁴, A. Cattai³⁶, J. Caudron²⁴, V. Cavaliere²⁹,
 E. Cavallaro¹⁴, M. Cavalli-Sforza¹⁴, V. Cavasinni^{71a,71b}, E. Celebi^{12b}, F. Ceradini^{74a,74b},
 L. Cerda Alberich¹⁷⁴, K. Cerny¹³⁰, A.S. Cerqueira^{80a}, A. Cerri¹⁵⁶, L. Cerrito^{73a,73b}, F. Cerutti¹⁸,
 A. Cervelli^{23b,23a}, S.A. Cetin^{12b}, Z. Chadi^{35a}, D. Chakraborty¹²¹, S.K. Chan⁵⁹, W.S. Chan¹²⁰, W.Y. Chan⁹⁰,
 J.D. Chapman³², B. Chargeishvili^{159b}, D.G. Charlton²¹, T.P. Charman⁹², C.C. Chau³⁴, S. Che¹²⁶,
 A. Chegwidden¹⁰⁶, S. Chekanov⁶, S.V. Chekulaev^{168a}, G.A. Chelkov^{79,aw}, M.A. Chelstowska³⁶, B. Chen⁷⁸,
 C. Chen^{60a}, C.H. Chen⁷⁸, H. Chen²⁹, J. Chen^{60a}, J. Chen³⁹, S. Chen¹³⁷, S.J. Chen^{15c}, X. Chen^{15b,av},
 Y. Chen⁸², Y-H. Chen⁴⁶, H.C. Cheng^{63a}, H.J. Cheng^{15a,15d}, A. Cheplakov⁷⁹, E. Cheremushkina¹²³,
 R. Cherkaoui El Moursli^{35e}, E. Cheu⁷, K. Cheung⁶⁴, T.J.A. Chevaléras¹⁴⁵, L. Chevalier¹⁴⁵, V. Chiarella⁵¹,
 G. Chiarelli^{71a}, G. Chiodini^{67a}, A.S. Chisholm^{36,21}, A. Chitan^{27b}, I. Chiu¹⁶³, Y.H. Chiu¹⁷⁶, M.V. Chizhov⁷⁹,
 K. Choi⁶⁵, A.R. Chomont^{72a,72b}, S. Chouridou¹⁶², Y.S. Chow¹²⁰, M.C. Chu^{63a}, X. Chu^{15a}, J. Chudoba¹⁴¹,
 A.J. Chuinard¹⁰³, J.J. Chwastowski⁸⁴, L. Chytka¹³⁰, K.M. Ciesla⁸⁴, D. Cinca⁴⁷, V. Cindro⁹¹, I.A. Cioara^{27b},
 A. Ciocio¹⁸, F. Ciroto^{69a,69b}, Z.H. Citron¹⁸⁰, M. Citterio^{68a}, D.A. Ciubotaru^{27b}, B.M. Ciungu¹⁶⁷,
 A. Clark⁵⁴, M.R. Clark³⁹, P.J. Clark⁵⁰, C. Clement^{45a,45b}, Y. Coadou¹⁰¹, M. Cobal^{66a,66c}, A. Coccaro^{55b},
 J. Cochran⁷⁸, H. Cohen¹⁶¹, A.E.C. Coimbra³⁶, L. Colasurdo¹¹⁹, B. Cole³⁹, A.P. Colijn¹²⁰, J. Collot⁵⁸,
 P. Conde Muiño^{140a,e}, E. Coniavitis⁵², S.H. Connell^{33b}, I.A. Connolly⁵⁷, S. Constantinescu^{27b},
 F. Conventi^{69a,ay}, A.M. Cooper-Sarkar¹³⁵, F. Cormier¹⁷⁵, K.J.R. Cormier¹⁶⁷, L.D. Corpe⁹⁴,
 M. Corradi^{72a,72b}, E.E. Corrigan⁹⁶, F. Corriveau^{103,ad}, A. Cortes-Gonzalez³⁶, M.J. Costa¹⁷⁴, F. Costanza⁵,
 D. Costanzo¹⁴⁹, G. Cowan⁹³, J.W. Cowley³², J. Crane¹⁰⁰, K. Cranmer¹²⁴, S.J. Crawley⁵⁷, R.A. Creager¹³⁷,
 S. Crépe-Renaudin⁵⁸, F. Crescioli¹³⁶, M. Cristinziani²⁴, V. Croft¹²⁰, G. Crosetti^{41b,41a}, A. Cueto⁵,
 T. Cuhadar Donszelmann¹⁴⁹, A.R. Cukierman¹⁵³, S. Czekierda⁸⁴, P. Czodrowski³⁶,
 M.J. Da Cunha Sargedas De Sousa^{60b}, J.V. Da Fonseca Pinto^{80b}, C. Da Via¹⁰⁰, W. Dabrowski^{83a},
 T. Dado^{28a}, S. Dahbi^{35e}, T. Dai¹⁰⁵, C. Dallapiccola¹⁰², M. Dam⁴⁰, G. D'amen^{23b,23a}, V. D'Amico^{74a,74b},
 J. Damp⁹⁹, J.R. Dandoy¹³⁷, M.F. Daneri³⁰, N.P. Dang¹⁸¹, N.D. Dann¹⁰⁰, M. Danninger¹⁷⁵, V. Dao³⁶,

G. Darbo^{55b}, O. Dartsis⁵, A. Dattagupta¹³¹, T. Daubney⁴⁶, S. D'Auria^{68a,68b}, W. Davey²⁴, C. David⁴⁶, T. Davidek¹⁴³, D.R. Davis⁴⁹, I. Dawson¹⁴⁹, K. De⁸, R. De Asmundis^{69a}, M. De Beurs¹²⁰, S. De Castro^{23b,23a}, S. De Cecco^{72a,72b}, N. De Groot¹¹⁹, P. de Jong¹²⁰, H. De la Torre¹⁰⁶, A. De Maria^{15c}, D. De Pedis^{72a}, A. De Salvo^{72a}, U. De Sanctis^{73a,73b}, M. De Santis^{73a,73b}, A. De Santo¹⁵⁶, K. De Vasconcelos Corga¹⁰¹, J.B. De Vivie De Regie¹³², C. Debenedetti¹⁴⁶, D.V. Dedovich⁷⁹, A.M. Deiana⁴², M. Del Gaudio^{41b,41a}, J. Del Peso⁹⁸, Y. Delabat Diaz⁴⁶, D. Delgove¹³², F. Deliot^{145,q}, C.M. Delitzsch⁷, M. Della Pietra^{69a,69b}, D. Della Volpe⁵⁴, A. Dell'Acqua³⁶, L. Dell'Asta^{73a,73b}, M. Delmastro⁵, C. Delporte¹³², P.A. Delsart⁵⁸, D.A. DeMarco¹⁶⁷, S. Demers¹⁸³, M. Demichev⁷⁹, G. Demontigny¹⁰⁹, S.P. Denisov¹²³, D. Denysiuk¹²⁰, L. D'Eramo¹³⁶, D. Derendarz⁸⁴, J.E. Derkaoui^{35d}, F. Derue¹³⁶, P. Dervan⁹⁰, K. Desch²⁴, C. Deterre⁴⁶, K. Dette¹⁶⁷, C. Deutsch²⁴, M.R. Devesa³⁰, P.O. Deviveiros³⁶, A. Dewhurst¹⁴⁴, S. Dhaliwal²⁶, F.A. Di Bello⁵⁴, A. Di Ciaccio^{73a,73b}, L. Di Ciaccio⁵, W.K. Di Clemente¹³⁷, C. Di Donato^{69a,69b}, A. Di Girolamo³⁶, G. Di Gregorio^{71a,71b}, B. Di Micco^{74a,74b}, R. Di Nardo¹⁰², K.F. Di Petrillo⁵⁹, R. Di Sipio¹⁶⁷, D. Di Valentino³⁴, C. Diaconu¹⁰¹, F.A. Dias⁴⁰, T. Dias Do Vale^{140a}, M.A. Diaz^{147a}, J. Dickinson¹⁸, E.B. Diehl¹⁰⁵, J. Dietrich¹⁹, S. Díez Cornell⁴⁶, A. Dimitrievska¹⁸, W. Ding^{15b}, J. Dingfelder²⁴, F. Dittus³⁶, F. Djama¹⁰¹, T. Djobava^{159b}, J.I. Djuvsland¹⁷, M.A.B. Do Vale^{80c}, M. Dobre^{27b}, D. Dodsworth²⁶, C. Doglioni⁹⁶, J. Dolejsi¹⁴³, Z. Dolezal¹⁴³, M. Donadelli^{80d}, B. Dong^{60c}, J. Donini³⁸, A. D'onofrio⁹², M. D'Onofrio⁹⁰, J. Dopke¹⁴⁴, A. Doria^{69a}, M.T. Dova⁸⁸, A.T. Doyle⁵⁷, E. Drechsler¹⁵², E. Dreyer¹⁵², T. Dreyer⁵³, A.S. Drobac¹⁷⁰, Y. Duan^{60b}, F. Dubinin¹¹⁰, M. Dubovsky^{28a}, A. Dubreuil⁵⁴, E. Duchovni¹⁸⁰, G. Duckeck¹¹⁴, A. Ducourthial¹³⁶, O.A. Ducu¹⁰⁹, D. Duda¹¹⁵, A. Dudarev³⁶, A.C. Dudder⁹⁹, E.M. Duffield¹⁸, L. Dufflot¹³², M. Dührssen³⁶, C. Dülsen¹⁸², M. Dumancic¹⁸⁰, A.E. Dumitriu^{27b}, A.K. Duncan⁵⁷, M. Dunford^{61a}, A. Duperrin¹⁰¹, H. Duran Yildiz^{4a}, M. Düren⁵⁶, A. Durglishvili^{159b}, D. Duschinger⁴⁸, B. Dutta⁴⁶, D. Duvnjak¹, G.I. Dyckes¹³⁷, M. Dyndal³⁶, S. Dysch¹⁰⁰, B.S. Dziedzic⁸⁴, K.M. Ecker¹¹⁵, R.C. Edgar¹⁰⁵, M.G. Eggleston⁴⁹, T. Eifert³⁶, G. Eigen¹⁷, K. Einsweiler¹⁸, T. Ekelof¹⁷², H. El Jarrari^{35e}, M. El Kacimi^{35c}, R. El Kosseifi¹⁰¹, V. Ellajosyula¹⁷², M. Ellert¹⁷², F. Ellinghaus¹⁸², A.A. Elliot⁹², N. Ellis³⁶, J. Elmsheuser²⁹, M. Elsing³⁶, D. Emelianov¹⁴⁴, A. Emerman³⁹, Y. Enari¹⁶³, M.B. Epland⁴⁹, J. Erdmann⁴⁷, A. Ereditato²⁰, M. Errenst³⁶, M. Escalier¹³², C. Escobar¹⁷⁴, O. Estrada Pastor¹⁷⁴, E. Etzion¹⁶¹, H. Evans⁶⁵, A. Ezhilov¹³⁸, F. Fabbri⁵⁷, L. Fabbri^{23b,23a}, V. Fabiani¹¹⁹, G. Facini⁹⁴, R.M. Faisca Rodrigues Pereira^{140a}, R.M. Fakhruudinov¹²³, S. Falciano^{72a}, P.J. Falke⁵, S. Falke⁵, J. Faltova¹⁴³, Y. Fang^{15a}, Y. Fang^{15a}, G. Fanourakis⁴⁴, M. Fanti^{68a,68b}, M. Faraj^{66a,66c}, A. Farbin⁸, A. Farilla^{74a}, E.M. Farina^{70a,70b}, T. Farooque¹⁰⁶, S. Farrell¹⁸, S.M. Farrington⁵⁰, P. Farthouat³⁶, F. Fassi^{35e}, P. Fassnacht³⁶, D. Fassouliotis⁹, M. Faucci Giannelli⁵⁰, W.J. Fawcett³², L. Fayard¹³², O.L. Fedin^{138,o}, W. Fedorko¹⁷⁵, M. Feickert⁴², S. Feigl¹³⁴, L. Felgioni¹⁰¹, A. Fell¹⁴⁹, C. Feng^{60b}, E.J. Feng³⁶, M. Feng⁴⁹, M.J. Fenton⁵⁷, A.B. Fenyuk¹²³, J. Ferrando⁴⁶, A. Ferrante¹⁷³, A. Ferrari¹⁷², P. Ferrari¹²⁰, R. Ferrari^{70a}, D.E. Ferreira de Lima^{61b}, A. Ferrer¹⁷⁴, D. Ferrere⁵⁴, C. Ferretti¹⁰⁵, F. Fiedler⁹⁹, A. Filipčič⁹¹, F. Filthaut¹¹⁹, K.D. Finelli²⁵, M.C.N. Fiolhais^{140a}, L. Fiorini¹⁷⁴, F. Fischer¹¹⁴, W.C. Fisher¹⁰⁶, I. Fleck¹⁵¹, P. Fleischmann¹⁰⁵, R.R.M. Fletcher¹³⁷, T. Flick¹⁸², B.M. Flierl¹¹⁴, L.F. Flores¹³⁷, L.R. Flores Castillo^{63a}, F.M. Follega^{75a,75b}, N. Fomin¹⁷, J.H. Foo¹⁶⁷, G.T. Forcolin^{75a,75b}, A. Formica¹⁴⁵, F.A. Förster¹⁴, A.C. Forti¹⁰⁰, A.G. Foster²¹, M.G. Foti¹³⁵, D. Fournier¹³², H. Fox⁸⁹, P. Francavilla^{71a,71b}, S. Francescato^{72a,72b}, M. Franchini^{23b,23a}, S. Franchino^{61a}, D. Francis³⁶, L. Franconi²⁰, M. Franklin⁵⁹, A.N. Fray⁹², B. Freund¹⁰⁹, W.S. Freund^{80b}, E.M. Freundlich⁴⁷, D.C. Frizzell¹²⁸, D. Froidevaux³⁶, J.A. Frost¹³⁵, C. Fukunaga¹⁶⁴, E. Fullana Torregrosa¹⁷⁴, E. Fumagalli^{55b,55a}, T. Fusayasu¹¹⁶, J. Fuster¹⁷⁴, A. Gabrielli^{23b,23a}, A. Gabrielli¹⁸, G.P. Gach^{83a}, S. Gadatsch⁵⁴, P. Gadow¹¹⁵, G. Gagliardi^{55b,55a}, L.G. Gagnon¹⁰⁹, C. Galea^{27b}, B. Galhardo^{140a}, G.E. Gallardo¹³⁵, E.J. Gallas¹³⁵, B.J. Gallop¹⁴⁴, G. Galster⁴⁰, R. Gamboa Goni⁹², K.K. Gan¹²⁶, S. Ganguly¹⁸⁰, J. Gao^{60a}, Y. Gao⁵⁰, Y.S. Gao^{31,1}, C. García¹⁷⁴, J.E. García Navarro¹⁷⁴, J.A. García Pascual^{15a}, C. Garcia-Argos⁵², M. Garcia-Sciveres¹⁸, R.W. Gardner³⁷, N. Garelli¹⁵³, S. Gargiulo⁵², V. Garonne¹³⁴, A. Gaudiello^{55b,55a}, G. Gaudio^{70a}, I.L. Gavrilenko¹¹⁰, A. Gavrilyuk¹¹¹, C. Gay¹⁷⁵, G. Gaycken⁴⁶, E.N. Gazis¹⁰, A.A. Geanta^{27b}, C.N.P. Gee¹⁴⁴, J. Geisen⁵³, M. Geisen⁹⁹,

M.P. Geisler^{61a}, C. Gemme^{55b}, M.H. Genest⁵⁸, C. Geng¹⁰⁵, S. Gentile^{72a,72b}, S. George⁹³, T. Gerialis⁴⁴, L.O. Gerlach⁵³, P. Gessinger-Befurt⁹⁹, G. Gessner⁴⁷, S. Ghasemi¹⁵¹, M. Ghasemi Bostanabad¹⁷⁶, M. Ghneimat²⁴, A. Ghosh¹³², A. Ghosh⁷⁷, B. Giacobbe^{23b}, S. Giagu^{72a,72b}, N. Giangiacomi^{23b,23a}, P. Giannetti^{71a}, A. Giannini^{69a,69b}, S.M. Gibson⁹³, M. Gignac¹⁴⁶, D. Gillberg³⁴, G. Gilles¹⁸², D.M. Gingrich^{3,ax}, M.P. Giordani^{66a,66c}, F.M. Giorgi^{23b}, P.F. Giraud¹⁴⁵, G. Giugliarelli^{66a,66c}, D. Giugni^{68a}, F. Giuli^{73a,73b}, S. Gkaitatzis¹⁶², I. Gkialas^{9,g}, E.L. Gkoukousis¹⁴, P. Gkoutoumis¹⁰, L.K. Gladilin¹¹³, C. Glasman⁹⁸, J. Glatzer¹⁴, P.C.F. Glaysheer⁴⁶, A. Glazov⁴⁶, M. Goblirsch-Kolb²⁶, S. Goldfarb¹⁰⁴, T. Golling⁵⁴, D. Golubkov¹²³, A. Gomes^{140a,140b}, R. Goncalves Gama⁵³, R. Gonçalo^{140a,140b}, G. Gonella⁵², L. Gonella²¹, A. Gongadze⁷⁹, F. Gonnella²¹, J.L. Gonski⁵⁹, S. González de la Hoz¹⁷⁴, S. Gonzalez-Sevilla⁵⁴, G.R. Gonzalvo Rodriguez¹⁷⁴, L. Goossens³⁶, P.A. Gorbounov¹¹¹, H.A. Gordon²⁹, B. Gorini³⁶, E. Gorini^{67a,67b}, A. Gorišek⁹¹, A.T. Goshaw⁴⁹, M.I. Gostkin⁷⁹, C.A. Gottardo¹¹⁹, M. Gouighri^{35b}, D. Goujdami^{35c}, A.G. Goussiou¹⁴⁸, N. Govender^{33b}, C. Goy⁵, E. Gozani¹⁶⁰, I. Grabowska-Bold^{83a}, E.C. Graham⁹⁰, J. Gramling¹⁷¹, E. Gramstad¹³⁴, S. Grancagnolo¹⁹, M. Grandi¹⁵⁶, V. Gratchev¹³⁸, P.M. Gravila^{27f}, F.G. Gravili^{67a,67b}, C. Gray⁵⁷, H.M. Gray¹⁸, C. Grefe²⁴, K. Gregersen⁹⁶, I.M. Gregor⁴⁶, P. Grenier¹⁵³, K. Grevtsov⁴⁶, C. Grieco¹⁴, N.A. Grieser¹²⁸, J. Griffiths⁸, A.A. Grillo¹⁴⁶, K. Grimm^{31,k}, S. Grinstein^{14,x}, J.-F. Grivaz¹³², S. Groh⁹⁹, E. Gross¹⁸⁰, J. Grosse-Knetter⁵³, Z.J. Grout⁹⁴, C. Grud¹⁰⁵, A. Grummer¹¹⁸, L. Guan¹⁰⁵, W. Guan¹⁸¹, J. Guenther³⁶, A. Guerguichon¹³², J.G.R. Guerrero Rojas¹⁷⁴, F. Guescini¹¹⁵, D. Guest¹⁷¹, R. Gugel⁵², T. Guillemin⁵, S. Guindon³⁶, U. Gul⁵⁷, J. Guo^{60c}, W. Guo¹⁰⁵, Y. Guo^{60a,s}, Z. Guo¹⁰¹, R. Gupta⁴⁶, S. Gurbuz^{12c}, G. Gustavino¹²⁸, P. Gutierrez¹²⁸, C. Gutsche⁹⁴, C. Guyot¹⁴⁵, C. Gwenlan¹³⁵, C.B. Gwilliam⁹⁰, A. Haas¹²⁴, C. Haber¹⁸, H.K. Hadavand⁸, N. Haddad^{35e}, A. Hadeef^{60a}, S. Hageböck³⁶, M. Hagihara¹⁶⁹, M. Haleem¹⁷⁷, J. Haley¹²⁹, G. Halladjian¹⁰⁶, G.D. Hallowell¹⁰¹, K. Hamacher¹⁸², P. Hamal¹³⁰, K. Hamano¹⁷⁶, H. Hamdaoui^{35e}, G.N. Hamity¹⁴⁹, K. Han^{60a,ak}, L. Han^{60a}, S. Han^{15a,15d}, K. Hanagaki^{81,v}, M. Hance¹⁴⁶, D.M. Handl¹¹⁴, B. Haney¹³⁷, R. Hankache¹³⁶, E. Hansen⁹⁶, J.B. Hansen⁴⁰, J.D. Hansen⁴⁰, M.C. Hansen²⁴, P.H. Hansen⁴⁰, E.C. Hanson¹⁰⁰, K. Hara¹⁶⁹, A.S. Hard¹⁸¹, T. Harenberg¹⁸², S. Harkusha¹⁰⁷, P.F. Harrison¹⁷⁸, N.M. Hartmann¹¹⁴, Y. Hasegawa¹⁵⁰, A. Hasib⁵⁰, S. Hassani¹⁴⁵, S. Haug²⁰, R. Hauser¹⁰⁶, L.B. Havener³⁹, M. Havranek¹⁴², C.M. Hawkes²¹, R.J. Hawkings³⁶, D. Hayden¹⁰⁶, C. Hayes¹⁵⁵, R.L. Hayes¹⁷⁵, C.P. Hays¹³⁵, J.M. Hays⁹², H.S. Hayward⁹⁰, S.J. Haywood¹⁴⁴, F. He^{60a}, M.P. Heath⁵⁰, V. Hedberg⁹⁶, L. Heelan⁸, S. Heer²⁴, K.K. Heidegger⁵², W.D. Heidorn⁷⁸, J. Heilman³⁴, S. Heim⁴⁶, T. Heim¹⁸, B. Heinemann^{46,as}, J.J. Heinrich¹³¹, L. Heinrich³⁶, C. Heinz⁵⁶, J. Hejbal¹⁴¹, L. Helary^{61b}, A. Held¹⁷⁵, S. Hellesund¹³⁴, C.M. Helling¹⁴⁶, S. Hellman^{45a,45b}, C. Helsens³⁶, R.C.W. Henderson⁸⁹, Y. Heng¹⁸¹, S. Henkelmann¹⁷⁵, A.M. Henriques Correia³⁶, G.H. Herbert¹⁹, H. Herde²⁶, V. Herget¹⁷⁷, Y. Hernández Jiménez^{33c}, H. Herr⁹⁹, M.G. Herrmann¹¹⁴, T. Herrmann⁴⁸, G. Herten⁵², R. Hertenberger¹¹⁴, L. Hervas³⁶, T.C. Herwig¹³⁷, G.G. Hesketh⁹⁴, N.P. Hessey^{168a}, A. Higashida¹⁶³, S. Higashino⁸¹, E. Higón-Rodriguez¹⁷⁴, K. Hildebrand³⁷, E. Hill¹⁷⁶, J.C. Hill³², K.K. Hill²⁹, K.H. Hiller⁴⁶, S.J. Hillier²¹, M. Hils⁴⁸, I. Hinchliffe¹⁸, F. Hinterkeuser²⁴, M. Hirose¹³³, S. Hirose⁵², D. Hirschbuehl¹⁸², B. Hiti⁹¹, O. Hladik¹⁴¹, D.R. Hlaluku^{33c}, X. Hoad⁵⁰, J. Hobbs¹⁵⁵, N. Hod¹⁸⁰, M.C. Hodgkinson¹⁴⁹, A. Hoecker³⁶, F. Hoenig¹¹⁴, D. Hohn⁵², D. Hohov¹³², T.R. Holmes³⁷, M. Holzbock¹¹⁴, L.B.A.H Hommels³², S. Honda¹⁶⁹, T. Honda⁸¹, T.M. Hong¹³⁹, A. Hönle¹¹⁵, B.H. Hooberman¹⁷³, W.H. Hopkins⁶, Y. Horii¹¹⁷, P. Horn⁴⁸, L.A. Horyn³⁷, A. Hostiuc¹⁴⁸, S. Hou¹⁵⁸, A. Hoummada^{35a}, J. Howarth¹⁰⁰, J. Hoya⁸⁸, M. Hrabovsky¹³⁰, J. Hrdinka⁷⁶, I. Hristova¹⁹, J. Hrivnac¹³², A. Hrynevich¹⁰⁸, T. Hryn'ova⁵, P.J. Hsu⁶⁴, S.-C. Hsu¹⁴⁸, Q. Hu²⁹, S. Hu^{60c}, Y. Huang^{15a}, Z. Hubacek¹⁴², F. Hubaut¹⁰¹, M. Huebner²⁴, F. Huegging²⁴, T.B. Huffman¹³⁵, M. Huhtinen³⁶, R.F.H. Hunter³⁴, P. Huo¹⁵⁵, A.M. Hupe³⁴, N. Huseynov^{79,af}, J. Huston¹⁰⁶, J. Huth⁵⁹, R. Hyneman¹⁰⁵, S. Hyrych^{28a}, G. Iacobucci⁵⁴, G. Iakovidis²⁹, I. Ibragimov¹⁵¹, L. Iconomidou-Fayard¹³², Z. Idrissi^{35e}, P.I. Inengo³⁶, R. Ignazzi⁴⁰, O. Igonkina^{120,z*}, R. Iguchi¹⁶³, T. Iizawa⁵⁴, Y. Ikegami⁸¹, M. Ikeno⁸¹, D. Iliadis¹⁶², N. Ilic¹¹⁹, F. Iltzsche⁴⁸, G. Introzzi^{70a,70b}, M. Iodice^{74a}, K. Iordanidou^{168a}, V. Ippolito^{72a,72b}, M.F. Isacson¹⁷², M. Ishino¹⁶³, M. Ishitsuka¹⁶⁵, W. Islam¹²⁹, C. Issever¹³⁵, S. Istin¹⁶⁰, F. Ito¹⁶⁹, J.M. Iturbe Ponce^{63a}, R. Iuppa^{75a,75b}, A. Ivina¹⁸⁰, H. Iwasaki⁸¹, J.M. Izen⁴³, V. Izzo^{69a},

P. Jacka¹⁴¹, P. Jackson¹, R.M. Jacobs²⁴, B.P. Jaeger¹⁵², V. Jain², G. Jäkel¹⁸², K.B. Jakobi⁹⁹, K. Jakobs⁵²,
 S. Jakobsen⁷⁶, T. Jakoubek¹⁴¹, J. Jamieson⁵⁷, K.W. Janas^{83a}, R. Jansky⁵⁴, J. Janssen²⁴, M. Janus⁵³,
 P.A. Janus^{83a}, G. Jarlskog⁹⁶, N. Javadov^{79,af}, T. Javůrek³⁶, M. Javurkova⁵², F. Jeanneau¹⁴⁵, L. Jeanty¹³¹,
 J. Jejelava^{159a,ag}, A. Jelinskas¹⁷⁸, P. Jenni^{52,a}, J. Jeong⁴⁶, N. Jeong⁴⁶, S. Jézéquel⁵, H. Ji¹⁸¹, J. Jia¹⁵⁵,
 H. Jiang⁷⁸, Y. Jiang^{60a}, Z. Jiang^{153,p}, S. Jiggins⁵², F.A. Jimenez Morales³⁸, J. Jimenez Pena¹¹⁵, S. Jin^{15c},
 A. Jinaru^{27b}, O. Jinnouchi¹⁶⁵, H. Jivan^{33c}, P. Johansson¹⁴⁹, K.A. Johns⁷, C.A. Johnson⁶⁵, K. Jon-And^{45a,45b},
 R.W.L. Jones⁸⁹, S.D. Jones¹⁵⁶, S. Jones⁷, T.J. Jones⁹⁰, J. Jongmanns^{61a}, P.M. Jorge^{140a}, J. Jovicevic³⁶,
 X. Ju¹⁸, J.J. Junggeburth¹¹⁵, A. Juste Rozas^{14,x}, A. Kaczmarska⁸⁴, M. Kado^{72a,72b}, H. Kagan¹²⁶,
 M. Kagan¹⁵³, C. Kahra⁹⁹, T. Kaji¹⁷⁹, E. Kajomovitz¹⁶⁰, C.W. Kalderon⁹⁶, A. Kaluza⁹⁹,
 A. Kamenshchikov¹²³, L. Kanjir⁹¹, Y. Kano¹⁶³, V.A. Kantserov¹¹², J. Kanzaki⁸¹, L.S. Kaplan¹⁸¹, D. Kar^{33c},
 M.J. Kareem^{168b}, S.N. Karpov⁷⁹, Z.M. Karpova⁷⁹, V. Kartvelishvili⁸⁹, A.N. Karyukhin¹²³, L. Kashif¹⁸¹,
 R.D. Kass¹²⁶, A. Kastanas^{45a,45b}, Y. Kataoka¹⁶³, C. Kato^{60d,60c}, J. Katzy⁴⁶, K. Kawade⁸², K. Kawagoe⁸⁷,
 T. Kawaguchi¹¹⁷, T. Kawamoto¹⁶³, G. Kawamura⁵³, E.F. Kay¹⁷⁶, V.F. Kazanin^{122b,122a}, R. Keeler¹⁷⁶,
 R. Kehoe⁴², J.S. Keller³⁴, E. Kellermann⁹⁶, D. Kelsey¹⁵⁶, J.J. Kempster²¹, J. Kendrick²¹, O. Kepka¹⁴¹,
 S. Kersten¹⁸², B.P. Kerševan⁹¹, S. Ketabchi Haghighat¹⁶⁷, M. Khader¹⁷³, F. Khalil-Zada¹³,
 M. Khandoga¹⁴⁵, A. Khanov¹²⁹, A.G. Kharlamov^{122b,122a}, T. Kharlamova^{122b,122a}, E.E. Khoda¹⁷⁵,
 A. Khodinov¹⁶⁶, T.J. Khoo⁵⁴, E. Khramov⁷⁹, J. Khubua^{159b}, S. Kido⁸², M. Kiehn⁵⁴, C.R. Kilby⁹³,
 Y.K. Kim³⁷, N. Kimura⁹⁴, O.M. Kind¹⁹, B.T. King^{90,*}, D. Kirchmeier⁴⁸, J. Kirk¹⁴⁴, A.E. Kiryunin¹¹⁵,
 T. Kishimoto¹⁶³, D.P. Kisliuk¹⁶⁷, V. Kitali⁴⁶, O. Kivernyk⁵, E. Kladiva^{28b,*}, T. Klapdor-Kleingrothaus⁵²,
 M. Klassen^{61a}, M.H. Klein¹⁰⁵, M. Klein⁹⁰, U. Klein⁹⁰, K. Kleinknecht⁹⁹, P. Klimek¹²¹, A. Klimentov²⁹,
 T. Klingl²⁴, T. Klioutchnikova³⁶, F.F. Klitzner¹¹⁴, P. Kluit¹²⁰, S. Kluth¹¹⁵, E. Kneringer⁷⁶,
 E.B.F.G. Knoop¹⁰¹, A. Knue⁵², D. Kobayashi⁸⁷, T. Kobayashi¹⁶³, M. Kobel⁴⁸, M. Kocian¹⁵³, P. Kodys¹⁴³,
 P.T. Koenig²⁴, T. Koffas³⁴, N.M. Köhler³⁶, T. Koi¹⁵³, M. Kolb^{61b}, I. Koletsou⁵, T. Komarek¹³⁰, T. Kondo⁸¹,
 N. Kondrashova^{60c}, K. Köneke⁵², A.C. König¹¹⁹, T. Kono¹²⁵, R. Konoplich^{124,an}, V. Konstantinides⁹⁴,
 N. Konstantinidis⁹⁴, B. Konya⁹⁶, R. Kopeliansky⁶⁵, S. Koperny^{83a}, K. Korcyl⁸⁴, K. Kordas¹⁶², G. Koren¹⁶¹,
 A. Korn⁹⁴, I. Korolkov¹⁴, E.V. Korolkova¹⁴⁹, N. Korotkova¹¹³, O. Kortner¹¹⁵, S. Kortner¹¹⁵, T. Kosek¹⁴³,
 V.V. Kostyukhin²⁴, A. Kotwal⁴⁹, A. Koulouris¹⁰, A. Kourkoumeli-Charalampidi^{70a,70b}, C. Kourkoumelis⁹,
 E. Kourlitis¹⁴⁹, V. Kouskoura²⁹, A.B. Kowalewska⁸⁴, R. Kowalewski¹⁷⁶, C. Kozakai¹⁶³, W. Kozanecki¹⁴⁵,
 A.S. Kozhin¹²³, V.A. Kramarenko¹¹³, G. Kramberger⁹¹, D. Krasnopevtsev^{60a}, M.W. Krasny¹³⁶,
 A. Krasznahorkay³⁶, D. Krauss¹¹⁵, J.A. Kremer^{83a}, J. Kretschmar⁹⁰, P. Krieger¹⁶⁷, F. Krieter¹¹⁴,
 A. Krishnan^{61b}, K. Krizka¹⁸, K. Kroeninger⁴⁷, H. Kroha¹¹⁵, J. Kroll¹⁴¹, J. Kroll¹³⁷, J. Krstic¹⁶,
 U. Kruchonak⁷⁹, H. Krüger²⁴, N. Krumnack⁷⁸, M.C. Kruse⁴⁹, J.A. Krzysiak⁸⁴, T. Kubota¹⁰⁴,
 O. Kuchinskaia¹⁶⁶, S. Kудay^{4b}, J.T. Kuechler⁴⁶, S. Kuehn³⁶, A. Kugel^{61a}, T. Kuhl⁴⁶, V. Kukhtin⁷⁹,
 R. Kukla¹⁰¹, Y. Kulchitsky^{107,aj}, S. Kuleshov^{147b}, Y.P. Kulinich¹⁷³, M. Kuna⁵⁸, T. Kunigo⁸⁵, A. Kupco¹⁴¹,
 T. Kupfer⁴⁷, O. Kuprash⁵², H. Kurashige⁸², L.L. Kurchaninov^{168a}, Y.A. Kurochkin¹⁰⁷, A. Kurova¹¹²,
 M.G. Kurth^{15a,15d}, E.S. Kuwertz³⁶, M. Kuze¹⁶⁵, A.K. Kvam¹⁴⁸, J. Kvita¹³⁰, T. Kwan¹⁰³, A. La Rosa¹¹⁵,
 L. La Rotonda^{41b,41a}, F. La Ruffa^{41b,41a}, C. Lacasta¹⁷⁴, F. Lacava^{72a,72b}, D.P.J. Lack¹⁰⁰, H. Lacker¹⁹,
 D. Lacour¹³⁶, E. Ladygin⁷⁹, R. Lafaye⁵, B. Laforge¹³⁶, T. Lagouri^{33c}, S. Lai⁵³, S. Lammers⁶⁵, W. Lampl⁷,
 C. Lampoudis¹⁶², E. Lançon²⁹, U. Landgraf⁵², M.P.J. Landon⁹², M.C. Lanfermann⁵⁴, V.S. Lang⁴⁶,
 J.C. Lange⁵³, R.J. Langenberg³⁶, A.J. Lankford¹⁷¹, F. Lanni²⁹, K. Lantzsches²⁴, A. Lanza^{70a},
 A. Lapertosa^{55b,55a}, S. Laplace¹³⁶, J.F. Laporte¹⁴⁵, T. Lari^{68a}, F. Lasagni Manghi^{23b,23a}, M. Lassnig³⁶,
 T.S. Lau^{63a}, A. Laudrain¹³², A. Laurier³⁴, M. Lavorgna^{69a,69b}, M. Lazzaroni^{68a,68b}, B. Le¹⁰⁴,
 E. Le Guirriec¹⁰¹, M. LeBlanc⁷, T. LeCompte⁶, F. Ledroit-Guillon⁵⁸, C.A. Lee²⁹, G.R. Lee¹⁷, L. Lee⁵⁹,
 S.C. Lee¹⁵⁸, S.J. Lee³⁴, B. Lefebvre^{168a}, M. Lefebvre¹⁷⁶, F. Legger¹¹⁴, C. Leggett¹⁸, K. Lehmann¹⁵²,
 N. Lehmann¹⁸², G. Lehmann Miotto³⁶, W.A. Leight⁴⁶, A. Leisos^{162,w}, M.A.L. Leite^{80d}, C.E. Leitgeb¹¹⁴,
 R. Leitner¹⁴³, D. Lellouch^{180,*}, K.J.C. Leney⁴², T. Lenz²⁴, B. Lenzi³⁶, R. Leone⁷, S. Leone^{71a},
 C. Leonidopoulos⁵⁰, A. Leopold¹³⁶, G. Lerner¹⁵⁶, C. Leroy¹⁰⁹, R. Les¹⁶⁷, C.G. Lester³², M. Levchenko¹³⁸,
 J. Levêque⁵, D. Levin¹⁰⁵, L.J. Levinson¹⁸⁰, D.J. Lewis²¹, B. Li^{15b}, B. Li¹⁰⁵, C-Q. Li^{60a}, F. Li^{60c}, H. Li^{60a},

H. Li^{60b}, J. Li^{60c}, K. Li¹⁵³, L. Li^{60c}, M. Li^{15a}, Q. Li^{15a,15d}, Q.Y. Li^{60a}, S. Li^{60d,60c}, X. Li⁴⁶, Y. Li⁴⁶, Z. Li^{60b}, Z. Liang^{15a}, B. Liberti^{73a}, A. Liblong¹⁶⁷, K. Lie^{63c}, S. Liem¹²⁰, C.Y. Lin³², K. Lin¹⁰⁶, T.H. Lin⁹⁹, R.A. Linck⁶⁵, J.H. Lindon²¹, A.L. Lioni⁵⁴, E. Lipeles¹³⁷, A. Lipniacka¹⁷, M. Lisovyi^{61b}, T.M. Liss^{173,au}, A. Lister¹⁷⁵, A.M. Litke¹⁴⁶, J.D. Little⁸, B. Liu^{78,ac}, B.L. Liu⁶, H.B. Liu²⁹, H. Liu¹⁰⁵, J.B. Liu^{60a}, J.K.K. Liu¹³⁵, K. Liu¹³⁶, M. Liu^{60a}, P. Liu¹⁸, Y. Liu^{15a,15d}, Y.L. Liu¹⁰⁵, Y.W. Liu^{60a}, M. Livan^{70a,70b}, A. Lleres⁵⁸, J. Llorente Merino^{15a}, S.L. Lloyd⁹², C.Y. Lo^{63b}, F. Lo Sterzo⁴², E.M. Lobodzinska⁴⁶, P. Loch⁷, S. Loffredo^{73a,73b}, T. Lohse¹⁹, K. Lohwasser¹⁴⁹, M. Lokajicek¹⁴¹, J.D. Long¹⁷³, R.E. Long⁸⁹, L. Longo³⁶, K.A. Looper¹²⁶, J.A. Lopez^{147b}, I. Lopez Paz¹⁰⁰, A. Lopez Solis¹⁴⁹, J. Lorenz¹¹⁴, N. Lorenzo Martinez⁵, M. Losada²², P.J. Lösel¹¹⁴, A. Lösle⁵², X. Lou⁴⁶, X. Lou^{15a}, A. Lounis¹³², J. Love⁶, P.A. Love⁸⁹, J.J. Lozano Bahilo¹⁷⁴, M. Lu^{60a}, Y.J. Lu⁶⁴, H.J. Lubatti¹⁴⁸, C. Luci^{72a,72b}, A. Lucotte⁵⁸, C. Luedtke⁵², F. Luehring⁶⁵, I. Luise¹³⁶, L. Luminari^{72a}, B. Lund-Jensen¹⁵⁴, M.S. Lutz¹⁰², D. Lynn²⁹, R. Lysak¹⁴¹, E. Lytken⁹⁶, F. Lyu^{15a}, V. Lyubushkin⁷⁹, T. Lyubushkina⁷⁹, H. Ma²⁹, L.L. Ma^{60b}, Y. Ma^{60b}, G. Maccarrone⁵¹, A. Macchiolo¹¹⁵, C.M. Macdonald¹⁴⁹, J. Machado Miguens¹³⁷, D. Madaffari¹⁷⁴, R. Madar³⁸, W.F. Mader⁴⁸, N. Madysa⁴⁸, J. Maeda⁸², K. Maekawa¹⁶³, S. Maeland¹⁷, T. Maeno²⁹, M. Maerker⁴⁸, A.S. Maevskiy¹¹³, V. Magerl⁵², N. Magini⁷⁸, D.J. Mahon³⁹, C. Maidantchik^{80b}, T. Maier¹¹⁴, A. Maio^{140a,140b,140d}, O. Majersky^{28a}, S. Majewski¹³¹, Y. Makida⁸¹, N. Makovec¹³², B. Malaescu¹³⁶, Pa. Malecki⁸⁴, V.P. Maleev¹³⁸, F. Malek⁵⁸, U. Mallik⁷⁷, D. Malon⁶, C. Malone³², S. Maltezos¹⁰, S. Malyukov³⁶, J. Mamuzic¹⁷⁴, G. Mancini⁵¹, I. Mandić⁹¹, L. Manhaes de Andrade Filho^{80a}, I.M. Maniatis¹⁶², J. Manjarres Ramos⁴⁸, K.H. Mankinen⁹⁶, A. Mann¹¹⁴, A. Manousos⁷⁶, B. Mansoulie¹⁴⁵, I. Mantos¹⁶², S. Manzoni¹²⁰, A. Marantis¹⁶², G. Marceca³⁰, L. Marchese¹³⁵, G. Marchiori¹³⁶, M. Marcisovsky¹⁴¹, C. Marcon⁹⁶, C.A. Marin Tobon³⁶, M. Marjanovic³⁸, Z. Marshall¹⁸, M.U.F. Martensson¹⁷², S. Marti-Garcia¹⁷⁴, C.B. Martin¹²⁶, T.A. Martin¹⁷⁸, V.J. Martin⁵⁰, B. Martin dit Latour¹⁷, L. Martinelli^{74a,74b}, M. Martinez^{14,x}, V.I. Martinez Outschoorn¹⁰², S. Martin-Haugh¹⁴⁴, V.S. Martoiu^{27b}, A.C. Martyniuk⁹⁴, A. Marzin³⁶, S.R. Maschek¹¹⁵, L. Masetti⁹⁹, T. Mashimo¹⁶³, R. Mashinistov¹¹⁰, J. Masik¹⁰⁰, A.L. Maslennikov^{122b,122a}, L.H. Mason¹⁰⁴, L. Massa^{73a,73b}, P. Massarotti^{69a,69b}, P. Mastrandrea^{71a,71b}, A. Mastroberardino^{41b,41a}, T. Masubuchi¹⁶³, D. Matakias¹⁰, A. Matic¹¹⁴, P. Mättig²⁴, J. Maurer^{27b}, B. Maček⁹¹, D.A. Maximov^{122b,122a}, R. Mazini¹⁵⁸, I. Maznas¹⁶², S.M. Mazza¹⁴⁶, S.P. Mc Kee¹⁰⁵, T.G. McCarthy¹¹⁵, L.I. McClymont⁹⁴, W.P. McCormack¹⁸, E.F. McDonald¹⁰⁴, J.A. McFayden³⁶, M.A. McKay⁴², K.D. McLean¹⁷⁶, S.J. McMahon¹⁴⁴, P.C. McNamara¹⁰⁴, C.J. McNicol¹⁷⁸, R.A. McPherson^{176,ad}, J.E. Mdhluhi^{33c}, Z.A. Meadows¹⁰², S. Meehan¹⁴⁸, T. Megy⁵², S. Mehlhase¹¹⁴, A. Mehta⁹⁰, T. Meideck⁵⁸, B. Meirose⁴³, D. Melini¹⁷⁴, B.R. Mellado Garcia^{33c}, J.D. Mellenthin⁵³, M. Melo^{28a}, F. Meloni⁴⁶, A. Melzer²⁴, S.B. Menary¹⁰⁰, E.D. Mendes Gouveia^{140a,140e}, L. Meng³⁶, X.T. Meng¹⁰⁵, S. Menke¹¹⁵, E. Meoni^{41b,41a}, S. Mergelmeyer¹⁹, S.A.M. Merkt¹³⁹, C. Merlassino²⁰, P. Mermod⁵⁴, L. Merola^{69a,69b}, C. Meroni^{68a}, O. Meshkov^{113,110}, J.K.R. Meshreki¹⁵¹, A. Messina^{72a,72b}, J. Metcalfe⁶, A.S. Mete¹⁷¹, C. Meyer⁶⁵, J. Meyer¹⁶⁰, J-P. Meyer¹⁴⁵, H. Meyer Zu Theenhausen^{61a}, F. Miano¹⁵⁶, M. Michetti¹⁹, R.P. Middleton¹⁴⁴, L. Mijović⁵⁰, G. Mikenberg¹⁸⁰, M. Mikestikova¹⁴¹, M. Mikuž⁹¹, H. Mildner¹⁴⁹, M. Milesi¹⁰⁴, A. Milic¹⁶⁷, D.A. Millar⁹², D.W. Miller³⁷, A. Milov¹⁸⁰, D.A. Milstead^{45a,45b}, R.A. Mina^{153,p}, A.A. Minaenko¹²³, M. Miñano Moya¹⁷⁴, I.A. Minashvili^{159b}, A.I. Mincer¹²⁴, B. Mindur^{83a}, M. Mineev⁷⁹, Y. Minegishi¹⁶³, Y. Ming¹⁸¹, L.M. Mir¹⁴, A. Mirto^{67a,67b}, K.P. Mistry¹³⁷, T. Mitani¹⁷⁹, J. Mitrevski¹¹⁴, V.A. Mitsou¹⁷⁴, M. Mittal^{60c}, A. Miucci²⁰, P.S. Miyagawa¹⁴⁹, A. Mizukami⁸¹, J.U. Mjörnmark⁹⁶, T. Mkrtychyan¹⁸⁴, M. Mlynarikova¹⁴³, T. Moa^{45a,45b}, K. Mochizuki¹⁰⁹, P. Mogg⁵², S. Mohapatra³⁹, R. Moles-Valls²⁴, M.C. Mondragon¹⁰⁶, K. Mönig⁴⁶, J. Monk⁴⁰, E. Monnier¹⁰¹, A. Montalbano¹⁵², J. Montejo Berlingen³⁶, M. Montella⁹⁴, F. Monticelli⁸⁸, S. Monzani^{68a}, N. Morange¹³², D. Moreno²², M. Moreno Llácer³⁶, C. Moreno Martinez¹⁴, P. Morettini^{55b}, M. Morgenstern¹²⁰, S. Morgenstern⁴⁸, D. Mori¹⁵², M. Morii⁵⁹, M. Morinaga¹⁷⁹, V. Morisbak¹³⁴, A.K. Morley³⁶, G. Mornacchi³⁶, A.P. Morris⁹⁴, L. Morvaj¹⁵⁵, P. Moschovakos³⁶, B. Moser¹²⁰, M. Mosidze^{159b}, T. Moskalets¹⁴⁵, H.J. Moss¹⁴⁹, J. Moss^{31,m}, K. Motohashi¹⁶⁵, E. Mountricha³⁶, E.J.W. Moyses¹⁰², S. Muanza¹⁰¹, J. Mueller¹³⁹, R.S.P. Mueller¹¹⁴, D. Muenstermann⁸⁹, G.A. Mullier⁹⁶,

J.L. Munoz Martinez¹⁴, F.J. Munoz Sanchez¹⁰⁰, P. Murin^{28b}, W.J. Murray^{178,144}, A. Murrone^{68a,68b}, M. Muškinja¹⁸, C. Mwewa^{33a}, A.G. Myagkov^{123,ao}, J. Myers¹³¹, M. Myska¹⁴², B.P. Nachman¹⁸, O. Nackenhurst⁴⁷, A.Nag Nag⁴⁸, K. Nagai¹³⁵, K. Nagano⁸¹, Y. Nagasaka⁶², M. Nagel⁵², E. Nagy¹⁰¹, A.M. Nairz³⁶, Y. Nakahama¹¹⁷, K. Nakamura⁸¹, T. Nakamura¹⁶³, I. Nakano¹²⁷, H. Nanjo¹³³, F. Napolitano^{61a}, R.F. Naranjo Garcia⁴⁶, R. Narayan⁴², I. Naryshkin¹³⁸, T. Naumann⁴⁶, G. Navarro²², H.A. Neal^{105,*}, P.Y. Nechaeva¹¹⁰, F. Nechansky⁴⁶, T.J. Neep²¹, A. Negri^{70a,70b}, M. Negrini^{23b}, C. Nellist⁵³, M.E. Nelson¹³⁵, S. Nemecek¹⁴¹, P. Nemethy¹²⁴, M. Nessi^{36,c}, M.S. Neubauer¹⁷³, M. Neumann¹⁸², P.R. Newman²¹, Y.S. Ng¹⁹, Y.W.Y. Ng¹⁷¹, H.D.N. Nguyen¹⁰¹, T. Nguyen Manh¹⁰⁹, E. Nibigira³⁸, R.B. Nickerson¹³⁵, R. Nicolaidou¹⁴⁵, D.S. Nielsen⁴⁰, J. Nielsen¹⁴⁶, N. Nikiforou¹¹, V. Nikolaenko^{123,ao}, I. Nikolic-Audit¹³⁶, K. Nikolopoulos²¹, P. Nilsson²⁹, H.R. Nindhito⁵⁴, Y. Ninomiya⁸¹, A. Nisati^{72a}, N. Nishu^{60c}, R. Nisius¹¹⁵, I. Nitsche⁴⁷, T. Nitta¹⁷⁹, T. Nobe¹⁶³, Y. Noguchi⁸⁵, I. Nomidis¹³⁶, M.A. Nomura²⁹, M. Nordberg³⁶, N. Norjoharuddeen¹³⁵, T. Novak⁹¹, O. Novgorodova⁴⁸, R. Novotny¹⁴², L. Nozka¹³⁰, K. Ntekas¹⁷¹, E. Nurse⁹⁴, F.G. Oakham^{34,ax}, H. Oberlack¹¹⁵, J. Ocariz¹³⁶, A. Ochi⁸², I. Ochoa³⁹, J.P. Ochoa-Ricoux^{147a}, K. O'Connor²⁶, S. Oda⁸⁷, S. Odaka⁸¹, S. Oerdek⁵³, A. Ogrodnik^{83a}, A. Oh¹⁰⁰, S.H. Oh⁴⁹, C.C. Ohm¹⁵⁴, H. Oide^{55b,55a}, M.L. Ojeda¹⁶⁷, H. Okawa¹⁶⁹, Y. Okazaki⁸⁵, Y. Okumura¹⁶³, T. Okuyama⁸¹, A. Olariu^{27b}, L.F. Oleiro Seabra^{140a}, S.A. Olivares Pino^{147a}, D. Oliveira Damazio²⁹, J.L. Oliver¹, M.J.R. Olsson¹⁷¹, A. Olszewski⁸⁴, J. Olszowska⁸⁴, D.C. O'Neil¹⁵², A. Onofre^{140a,140e}, K. Onogi¹¹⁷, P.U.E. Onyisi¹¹, H. Oppen¹³⁴, M.J. Oreglia³⁷, G.E. Orellana⁸⁸, D. Orestano^{74a,74b}, N. Orlando¹⁴, R.S. Orr¹⁶⁷, V. O'Shea⁵⁷, R. Ospanov^{60a}, G. Otero y Garzon³⁰, H. Otono⁸⁷, P.S. Ott^{61a}, M. Ouchrif^{35d}, J. Ouellette²⁹, F. Ould-Saada¹³⁴, A. Ouraou¹⁴⁵, Q. Ouyang^{15a}, M. Owen⁵⁷, R.E. Owen²¹, V.E. Ozcan^{12c}, N. Ozturk⁸, J. Pacalt¹³⁰, H.A. Pacey³², K. Pachal⁴⁹, A. Pacheco Pages¹⁴, C. Padilla Aranda¹⁴, S. Pagan Griso¹⁸, M. Paganini¹⁸³, G. Palacino⁶⁵, S. Palazzo⁵⁰, S. Palestini³⁶, M. Palka^{83b}, D. Pallin³⁸, I. Panagoulas¹⁰, C.E. Pandini³⁶, J.G. Panduro Vazquez⁹³, P. Pani⁴⁶, G. Panizzo^{66a,66c}, L. Paolozzi⁵⁴, C. Papadatos¹⁰⁹, K. Papageorgiou^{9,g}, A. Paramonov⁶, D. Paredes Hernandez^{63b}, S.R. Paredes Saenz¹³⁵, B. Parida¹⁶⁶, T.H. Park¹⁶⁷, A.J. Parker⁸⁹, M.A. Parker³², F. Parodi^{55b,55a}, E.W.P. Parrish¹²¹, J.A. Parsons³⁹, U. Parzefall⁵², L. Pascual Dominguez¹³⁶, V.R. Pascuzzi¹⁶⁷, J.M.P. Pasner¹⁴⁶, E. Pasqualucci^{72a}, S. Passaggio^{55b}, F. Pastore⁹³, P. Pasuwan^{45a,45b}, S. Pataraja⁹⁹, J.R. Pater¹⁰⁰, A. Pathak¹⁸¹, T. Pauly³⁶, B. Pearson¹¹⁵, M. Pedersen¹³⁴, L. Pedraza Diaz¹¹⁹, R. Pedro^{140a}, T. Peiffer⁵³, S.V. Peleganchuk^{122b,122a}, O. Penc¹⁴¹, H. Peng^{60a}, B.S. Peralva^{80a}, M.M. Perego¹³², A.P. Pereira Peixoto^{140a}, D.V. Perepelitsa²⁹, F. Peri¹⁹, L. Perini^{68a,68b}, H. Pernegger³⁶, S. Perrella^{69a,69b}, K. Peters⁴⁶, R.F.Y. Peters¹⁰⁰, B.A. Petersen³⁶, T.C. Petersen⁴⁰, E. Petit¹⁰¹, A. Petridis¹, C. Petridou¹⁶², P. Petroff¹³², M. Petrov¹³⁵, F. Petrucci^{74a,74b}, M. Pettee¹⁸³, N.E. Pettersson¹⁰², K. Petukhova¹⁴³, A. Peyaud¹⁴⁵, R. Pezoa^{147b}, L. Pezzotti^{70a,70b}, T. Pham¹⁰⁴, F.H. Phillips¹⁰⁶, P.W. Phillips¹⁴⁴, M.W. Phipps¹⁷³, G. Piacquadio¹⁵⁵, E. Pianori¹⁸, A. Picazio¹⁰², R.H. Pickles¹⁰⁰, R. Piegaia³⁰, D. Pietreanu^{27b}, J.E. Pilcher³⁷, A.D. Pilkington¹⁰⁰, M. Pinamonti^{73a,73b}, J.L. Pinfold³, M. Pitt¹⁸⁰, L. Pizzimento^{73a,73b}, M.-A. Pleier²⁹, V. Pleskot¹⁴³, E. Plotnikova⁷⁹, P. Podberezko^{122b,122a}, R. Poettgen⁹⁶, R. Poggi⁵⁴, L. Poggioli¹³², I. Pogrebnyak¹⁰⁶, D. Pohl²⁴, I. Pokharel⁵³, G. Polesello^{70a}, A. Poley¹⁸, A. Policicchio^{72a,72b}, R. Polifka¹⁴³, A. Polini^{23b}, C.S. Pollard⁴⁶, V. Polychronakos²⁹, D. Ponomarenko¹¹², L. Pontecorvo³⁶, S. Popa^{27a}, G.A. Popeneciu^{27d}, D.M. Portillo Quintero⁵⁸, S. Pospisil¹⁴², K. Potamianos⁴⁶, I.N. Potrap⁷⁹, C.J. Potter³², H. Potti¹¹, T. Poulsen⁹⁶, J. Poveda³⁶, T.D. Powell¹⁴⁹, G. Pownall⁴⁶, M.E. Pozo Astigarraga³⁶, P. Pralavorio¹⁰¹, S. Prell⁷⁸, D. Price¹⁰⁰, M. Primavera^{67a}, S. Prince¹⁰³, M.L. Proffitt¹⁴⁸, N. Proklova¹¹², K. Prokofiev^{63c}, F. Prokoshin⁷⁹, S. Protopopescu²⁹, J. Proudfoot⁶, M. Przybycien^{83a}, D. Pudzha¹³⁸, A. Puri¹⁷³, P. Puzo¹³², J. Qian¹⁰⁵, Y. Qin¹⁰⁰, A. Quadt⁵³, M. Queitsch-Maitland⁴⁶, A. Qureshi¹, P. Rados¹⁰⁴, F. Ragusa^{68a,68b}, G. Rahal⁹⁷, J.A. Raine⁵⁴, S. Rajagopalan²⁹, A. Ramirez Morales⁹², K. Ran^{15a,15d}, T. Rashid¹³², S. Raspopov⁵, D.M. Rauch⁴⁶, F. Rauscher¹¹⁴, S. Rave⁹⁹, B. Ravina¹⁴⁹, I. Ravinovich¹⁸⁰, J.H. Rawling¹⁰⁰, M. Raymond³⁶, A.L. Read¹³⁴, N.P. Readioff⁵⁸, M. Reale^{67a,67b}, D.M. Rebuffi^{70a,70b}, A. Redelbach¹⁷⁷, G. Redlinger²⁹, K. Reeves⁴³, L. Rehnisch¹⁹, J. Reichert¹³⁷, D. Reikher¹⁶¹, A. Reiss⁹⁹, A. Rej¹⁵¹, C. Rembser³⁶,

M. Renda^{27b}, M. Rescigno^{72a}, S. Resconi^{68a}, E.D. Resseguie¹³⁷, S. Rettie¹⁷⁵, E. Reynolds²¹,
 O.L. Rezanova^{122b,122a}, P. Reznicek¹⁴³, E. Ricci^{75a,75b}, R. Richter¹¹⁵, S. Richter⁴⁶, E. Richter-Was^{83b},
 O. Ricken²⁴, M. Ridel¹³⁶, P. Rieck¹¹⁵, C.J. Riegel¹⁸², O. Rifki⁴⁶, M. Rijssenbeek¹⁵⁵, A. Rimoldi^{70a,70b},
 M. Rimoldi⁴⁶, L. Rinaldi^{23b}, G. Ripellino¹⁵⁴, B. Ristić⁸⁹, I. Riu¹⁴, J.C. Rivera Vergara¹⁷⁶, F. Rizatdinova¹²⁹,
 E. Rizvi⁹², C. Rizzi³⁶, R.T. Roberts¹⁰⁰, S.H. Robertson^{103,ad}, M. Robin⁴⁶, D. Robinson³²,
 J.E.M. Robinson⁴⁶, C.M. Robles Gajardo^{147b}, A. Robson⁵⁷, E. Rocco⁹⁹, C. Roda^{71a,71b},
 S. Rodriguez Bosca¹⁷⁴, A. Rodriguez Perez¹⁴, D. Rodriguez Rodriguez¹⁷⁴, A.M. Rodríguez Vera^{168b},
 S. Roe³⁶, O. Røhne¹³⁴, R. Röhrig¹¹⁵, C.P.A. Roland⁶⁵, J. Roloff⁵⁹, A. Romaniouk¹¹², M. Romano^{23b,23a},
 N. Rompotis⁹⁰, M. Ronzani¹²⁴, L. Roos¹³⁶, S. Rosati^{72a}, K. Rosbach⁵², G. Rosin¹⁰², B.J. Rosser¹³⁷,
 E. Rossi⁴⁶, E. Rossi^{74a,74b}, E. Rossi^{69a,69b}, L.P. Rossi^{55b}, L. Rossini^{68a,68b}, R. Rosten¹⁴, M. Rotaru^{27b},
 J. Rothberg¹⁴⁸, D. Rousseau¹³², G. Rovelli^{70a,70b}, A. Roy¹¹, D. Roy^{33c}, A. Rozanov¹⁰¹, Y. Rozen¹⁶⁰,
 X. Ruan^{33c}, F. Rubbo¹⁵³, F. Rühr⁵², A. Ruiz-Martinez¹⁷⁴, A. Rummeler³⁶, Z. Rurikova⁵², N.A. Rusakovich⁷⁹,
 H.L. Russell¹⁰³, L. Rustige^{38,47}, J.P. Rutherford⁷, E.M. Rüttinger^{46,j}, Y.F. Ryabov¹³⁸, M. Rybar³⁹,
 G. Rybkin¹³², E.B. Rye¹³⁴, A. Ryzhov¹²³, G.F. Rzehorz⁵³, P. Sabatini⁵³, G. Sabato¹²⁰, S. Sacerdoti¹³²,
 H.F.W. Sadrozinski¹⁴⁶, R. Sadykov⁷⁹, F. Safai Tehrani^{72a}, B. Safarzadeh Samani¹⁵⁶, P. Saha¹²¹, S. Saha¹⁰³,
 M. Sahinsoy^{61a}, A. Sahu¹⁸², M. Saimpert⁴⁶, M. Saito¹⁶³, T. Saito¹⁶³, H. Sakamoto¹⁶³, A. Sakharov^{124,an},
 D. Salamani⁵⁴, G. Salamanna^{74a,74b}, J.E. Salazar Loyola^{147b}, P.H. Sales De Bruin¹⁷², A. Salnikov¹⁵³,
 J. Salt¹⁷⁴, D. Salvatore^{41b,41a}, F. Salvatore¹⁵⁶, A. Salvucci^{63a,63b,63c}, A. Salzburger³⁶, J. Samarati³⁶,
 D. Sammel⁵², D. Sampsonidis¹⁶², D. Sampsonidou¹⁶², J. Sánchez¹⁷⁴, A. Sanchez Pineda^{66a,66c},
 H. Sandaker¹³⁴, C.O. Sander⁴⁶, I.G. Sanderswood⁸⁹, M. Sandhoff¹⁸², C. Sandoval²², D.P.C. Sankey¹⁴⁴,
 M. Sannino^{55b,55a}, Y. Sano¹¹⁷, A. Sansoni⁵¹, C. Santoni³⁸, H. Santos^{140a,140b}, S.N. Santpur¹⁸, A. Santra¹⁷⁴,
 A. Sapronov⁷⁹, J.G. Saraiva^{140a,140d}, O. Sasaki⁸¹, K. Sato¹⁶⁹, E. Sauvan⁵, P. Savard^{167,ax}, N. Savic¹¹⁵,
 R. Sawada¹⁶³, C. Sawyer¹⁴⁴, L. Sawyer^{95,al}, C. Sbarra^{23b}, A. Sbrizzi^{23a}, T. Scanlon⁹⁴, J. Schaarschmidt¹⁴⁸,
 P. Schacht¹¹⁵, B.M. Schachtner¹¹⁴, D. Schaefer³⁷, L. Schaefer¹³⁷, J. Schaeffer⁹⁹, S. Schaepe³⁶, U. Schäfer⁹⁹,
 A.C. Schaffer¹³², D. Schaile¹¹⁴, R.D. Schamberger¹⁵⁵, N. Scharmberg¹⁰⁰, V.A. Schegelsky¹³⁸,
 D. Scheirich¹⁴³, F. Schenck¹⁹, M. Schernau¹⁷¹, C. Schiavi^{55b,55a}, S. Schier¹⁴⁶, L.K. Schildgen²⁴,
 Z.M. Schillaci²⁶, E.J. Schioppa³⁶, M. Schioppa^{41b,41a}, K.E. Schleicher⁵², S. Schlenker³⁶,
 K.R. Schmidt-Sommerfeld¹¹⁵, K. Schmieden³⁶, C. Schmitt⁹⁹, S. Schmitt⁴⁶, S. Schmitz⁹⁹,
 J.C. Schmoedel⁴⁶, U. Schnoor⁵², L. Schoeffel¹⁴⁵, A. Schoening^{61b}, P.G. Scholer⁵², E. Schopf¹³⁵,
 M. Schott⁹⁹, J.F.P. Schouwenberg¹¹⁹, J. Schovancova³⁶, S. Schramm⁵⁴, F. Schroeder¹⁸², A. Schulte⁹⁹,
 H-C. Schultz-Coulon^{61a}, M. Schumacher⁵², B.A. Schumm¹⁴⁶, Ph. Schune¹⁴⁵, A. Schwartzman¹⁵³,
 T.A. Schwarz¹⁰⁵, Ph. Schwemling¹⁴⁵, R. Schwienhorst¹⁰⁶, A. Sciandra¹⁴⁶, G. Sciolla²⁶, M. Scodreggio⁴⁶,
 M. Scornajenghi^{41b,41a}, F. Scuri^{71a}, F. Scutti¹⁰⁴, L.M. Scyboz¹¹⁵, C.D. Sebastiani^{72a,72b}, P. Seema¹⁹,
 S.C. Seidel¹¹⁸, A. Seiden¹⁴⁶, T. Seiss³⁷, J.M. Seixas^{80b}, G. Sekhniaidze^{69a}, K. Sekhon¹⁰⁵, S.J. Sekula⁴²,
 N. Semprini-Cesari^{23b,23a}, S. Sen⁴⁹, S. Senkin³⁸, C. Serfon⁷⁶, L. Serin¹³², L. Serkin^{66a,66b}, M. Sessa^{60a},
 H. Severini¹²⁸, F. Sforza¹⁷⁰, A. Sfyrla⁵⁴, E. Shabalina⁵³, J.D. Shahinian¹⁴⁶, N.W. Shaikh^{45a,45b},
 D. Shaked Renous¹⁸⁰, L.Y. Shan^{15a}, R. Shang¹⁷³, J.T. Shank²⁵, M. Shapiro¹⁸, A. Sharma¹³⁵, A.S. Sharma¹,
 P.B. Shatalov¹¹¹, K. Shaw¹⁵⁶, S.M. Shaw¹⁰⁰, A. Shcherbakova¹³⁸, Y. Shen¹²⁸, N. Sherafati³⁴,
 A.D. Sherman²⁵, P. Sherwood⁹⁴, L. Shi^{158,at}, S. Shimizu⁸¹, C.O. Shimmin¹⁸³, Y. Shimogama¹⁷⁹,
 M. Shimojima¹¹⁶, I.P.J. Shipsey¹³⁵, S. Shirabe⁸⁷, M. Shiyakova^{79,aa}, J. Shlomi¹⁸⁰, A. Shmeleva¹¹⁰,
 M.J. Shochet³⁷, J. Shojaii¹⁰⁴, D.R. Shope¹²⁸, S. Shrestha¹²⁶, E.M. Shrif^{33c}, E. Shulga¹⁸⁰, P. Sicho¹⁴¹,
 A.M. Sickles¹⁷³, P.E. Sidebo¹⁵⁴, E. Sideras Haddad^{33c}, O. Sidiropoulou³⁶, A. Sidoti^{23b,23a}, F. Siegert⁴⁸,
 Dj. Sijacki¹⁶, M. Silva Jr.¹⁸¹, M.V. Silva Oliveira^{80a}, S.B. Silverstein^{45a}, S. Simion¹³², E. Simioni⁹⁹,
 R. Simoniello⁹⁹, S. Simsek^{12b}, P. Sinervo¹⁶⁷, V. Sinetckii^{113,110}, N.B. Sinev¹³¹, M. Sioli^{23b,23a}, I. Siral¹⁰⁵,
 S.Yu. Sivoklov¹¹³, J. Sjölin^{45a,45b}, E. Skorda⁹⁶, P. Skubic¹²⁸, M. Slawinska⁸⁴, K. Sliwa¹⁷⁰, R. Slovak¹⁴³,
 V. Smakhtin¹⁸⁰, B.H. Smart¹⁴⁴, J. Smiesko^{28a}, N. Smirnov¹¹², S.Yu. Smirnov¹¹², Y. Smirnov¹¹²,
 L.N. Smirnova^{113,t}, O. Smirnova⁹⁶, J.W. Smith⁵³, M. Smizanska⁸⁹, K. Smolek¹⁴², A. Smykiewicz⁸⁴,
 A.A. Snesarev¹¹⁰, H.L. Snoek¹²⁰, I.M. Snyder¹³¹, S. Snyder²⁹, R. Sobie^{176,ad}, A.M. Soffa¹⁷¹, A. Soffer¹⁶¹,

A. Sjøgaard⁵⁰, F. Sohns⁵³, C.A. Solans Sanchez³⁶, E.Yu. Soldatov¹¹², U. Soldevila¹⁷⁴, A.A. Solodkov¹²³,
 A. Soloshenko⁷⁹, O.V. Solovyanov¹²³, V. Solovyev¹³⁸, P. Sommer¹⁴⁹, H. Son¹⁷⁰, W. Song¹⁴⁴,
 W.Y. Song^{168b}, A. Sopczak¹⁴², F. Sopkova^{28b}, C.L. Sotiropoulou^{71a,71b}, S. Sottocornola^{70a,70b},
 R. Soualah^{66a,66c,f}, A.M. Soukharev^{122b,122a}, D. South⁴⁶, S. Spagnolo^{67a,67b}, M. Spalla¹¹⁵,
 M. Spangenberg¹⁷⁸, F. Spanò⁹³, D. Sperlich⁵², T.M. Spieker^{61a}, R. Spighi^{23b}, G. Spigo³⁶, M. Spina¹⁵⁶,
 D.P. Spiteri⁵⁷, M. Spousta¹⁴³, A. Stabile^{68a,68b}, B.L. Stamas¹²¹, R. Stamen^{61a}, M. Stamenkovic¹²⁰,
 E. Stanecka⁸⁴, R.W. Stanek⁶, B. Stanislaus¹³⁵, M.M. Stanitzki⁴⁶, M. Stankaityte¹³⁵, B. Stapf¹²⁰,
 E.A. Starchenko¹²³, G.H. Stark¹⁴⁶, J. Stark⁵⁸, S.H. Stark⁴⁰, P. Staroba¹⁴¹, P. Starovoitov^{61a}, S. Stärz¹⁰³,
 R. Staszewski⁸⁴, G. Stavropoulos⁴⁴, M. Stegler⁴⁶, P. Steinberg²⁹, A.L. Steinhebel¹³¹, B. Stelzer¹⁵²,
 H.J. Stelzer¹³⁹, O. Stelzer-Chilton^{168a}, H. Stenzel⁵⁶, T.J. Stevenson¹⁵⁶, G.A. Stewart³⁶, M.C. Stockton³⁶,
 G. Stoicea^{27b}, M. Stolarski^{140a}, P. Stolte⁵³, S. Stonjek¹¹⁵, A. Straessner⁴⁸, J. Strandberg¹⁵⁴,
 S. Strandberg^{45a,45b}, M. Strauss¹²⁸, P. Strizenec^{28b}, R. Ströhmer¹⁷⁷, D.M. Strom¹³¹, R. Stroynowski⁴²,
 A. Strubig⁵⁰, S.A. Stucci²⁹, B. Stugu¹⁷, J. Stupak¹²⁸, N.A. Styles⁴⁶, D. Su¹⁵³, S. Suchek^{61a}, V.V. Sulin¹¹⁰,
 M.J. Sullivan⁹⁰, D.M.S. Sultan⁵⁴, S. Sultansoy^{4c}, T. Sumida⁸⁵, S. Sun¹⁰⁵, X. Sun³, K. Suruliz¹⁵⁶,
 C.J.E. Suster¹⁵⁷, M.R. Sutton¹⁵⁶, S. Suzuki⁸¹, M. Svatos¹⁴¹, M. Swiatlowski³⁷, S.P. Swift², T. Swirski¹⁷⁷,
 A. Sydorenko⁹⁹, I. Sykora^{28a}, M. Sykora¹⁴³, T. Sykora¹⁴³, D. Ta⁹⁹, K. Tackmann^{46,y}, J. Taenzer¹⁶¹,
 A. Taffard¹⁷¹, R. Tafirout^{168a}, H. Takai²⁹, R. Takashima⁸⁶, K. Takeda⁸², T. Takeshita¹⁵⁰, E.P. Takeva⁵⁰,
 Y. Takubo⁸¹, M. Talby¹⁰¹, A.A. Talyshev^{122b,122a}, N.M. Tamir¹⁶¹, J. Tanaka¹⁶³, M. Tanaka¹⁶⁵, R. Tanaka¹³²,
 S. Tapia Araya¹⁷³, S. Tapprogge⁹⁹, A. Tarek Abouelfadl Mohamed¹³⁶, S. Tarem¹⁶⁰, G. Tarna^{27b,b},
 G.F. Tartarelli^{68a}, P. Tas¹⁴³, M. Tasevsky¹⁴¹, T. Tashiro⁸⁵, E. Tassi^{41b,41a}, A. Tavares Delgado^{140a,140b},
 Y. Tayalati^{35e}, A.J. Taylor⁵⁰, G.N. Taylor¹⁰⁴, W. Taylor^{168b}, A.S. Tee⁸⁹, R. Teixeira De Lima¹⁵³,
 P. Teixeira-Dias⁹³, H. Ten Kate³⁶, J.J. Teoh¹²⁰, S. Terada⁸¹, K. Terashi¹⁶³, J. Terron⁹⁸, S. Terzo¹⁴,
 M. Testa⁵¹, R.J. Teuscher^{167,ad}, S.J. Thais¹⁸³, T. Thevenaux-Pelzer⁴⁶, F. Thiele⁴⁰, D.W. Thomas⁹³,
 J.O. Thomas⁴², J.P. Thomas²¹, A.S. Thompson⁵⁷, P.D. Thompson²¹, L.A. Thomsen¹⁸³, E. Thomson¹³⁷,
 E.J. Thorpe⁹², Y. Tian³⁹, R.E. Ticse Torres⁵³, V.O. Tikhomirov^{110,ap}, Yu.A. Tikhonov^{122b,122a},
 S. Timoshenko¹¹², P. Tipton¹⁸³, S. Tisserant¹⁰¹, K. Todome^{23b,23a}, S. Todorova-Nova⁵, S. Todt⁴⁸, J. Tojo⁸⁷,
 S. Tokár^{28a}, K. Tokushuku⁸¹, E. Tolley¹²⁶, K.G. Tomiwa^{33c}, M. Tomoto¹¹⁷, L. Tompkins^{153,p}, K. Toms¹¹⁸,
 B. Tong⁵⁹, P. Tornambe¹⁰², E. Torrence¹³¹, H. Torres⁴⁸, E. Torró Pastor¹⁴⁸, C. Toscirì¹³⁵, J. Toth^{101,ab},
 D.R. Tovey¹⁴⁹, A. Traeet¹⁷, C.J. Treado¹²⁴, T. Trefzger¹⁷⁷, F. Tresoldi¹⁵⁶, A. Tricoli²⁹, I.M. Trigger^{168a},
 S. Trincz-Duvoid¹³⁶, W. Trischuk¹⁶⁷, B. Trocmé⁵⁸, A. Trofymov¹³², C. Troncon^{68a}, M. Trovatelli¹⁷⁶,
 F. Trovato¹⁵⁶, L. Truong^{33b}, M. Trzebinski⁸⁴, A. Trzupek⁸⁴, F. Tsai⁴⁶, J.C.-L. Tseng¹³⁵, P.V. Tsiareshka^{107,aj},
 A. Tsirigotis¹⁶², N. Tsirintanis⁹, V. Tsiskaridze¹⁵⁵, E.G. Tskhadadze^{159a}, M. Tsopoulou¹⁶²,
 I.I. Tsukerman¹¹¹, V. Tsulaia¹⁸, S. Tsuno⁸¹, D. Tsybychev¹⁵⁵, Y. Tu^{63b}, A. Tudorache^{27b}, V. Tudorache^{27b},
 T.T. Tulbure^{27a}, A.N. Tuna⁵⁹, S. Turchikhin⁷⁹, D. Turgeman¹⁸⁰, I. Turk Cakir^{4b,u}, R.J. Turner²¹,
 R.T. Turra^{68a}, P.M. Tuts³⁹, S. Tzamarias¹⁶², E. Tzovara⁹⁹, G. Ucchielli⁴⁷, K. Uchida¹⁶³, I. Ueda⁸¹,
 M. Ughetto^{45a,45b}, F. Ukegawa¹⁶⁹, G. Unal³⁶, A. Undrus²⁹, G. Unel¹⁷¹, F.C. Ungaro¹⁰⁴, Y. Unno⁸¹,
 K. Uno¹⁶³, J. Urban^{28b}, P. Urquijo¹⁰⁴, G. Usai⁸, J. Usui⁸¹, Z. Uysal^{12d}, L. Vacavant¹⁰¹, V. Vacek¹⁴²,
 B. Vachon¹⁰³, K.O.H. Vadla¹³⁴, A. Vaidya⁹⁴, C. Valderanis¹¹⁴, E. Valdes Santurio^{45a,45b}, M. Valente⁵⁴,
 S. Valentineti^{23b,23a}, A. Valero¹⁷⁴, L. Valéry⁴⁶, R.A. Vallance²¹, A. Vallier³⁶, J.A. Valls Ferrer¹⁷⁴,
 T.R. Van Daalen¹⁴, P. Van Gemmeren⁶, I. Van Vulpen¹²⁰, M. Vanadia^{73a,73b}, W. Vandelli³⁶,
 A. Vaniachine¹⁶⁶, D. Vannicola^{72a,72b}, R. Vari^{72a}, E.W. Varnes⁷, C. Varni^{55b,55a}, T. Varol⁴²,
 D. Varouchas¹³², K.E. Varvell¹⁵⁷, M.E. Vasile^{27b}, G.A. Vasquez¹⁷⁶, J.G. Vasquez¹⁸³, F. Vazeille³⁸,
 D. Vazquez Furelos¹⁴, T. Vazquez Schroeder³⁶, J. Veatch⁵³, V. Vecchio^{74a,74b}, M.J. Veen¹²⁰,
 L.M. Veloce¹⁶⁷, F. Veloso^{140a,140c}, S. Veneziano^{72a}, A. Ventura^{67a,67b}, N. Venturi³⁶, A. Verbytskyi¹¹⁵,
 V. Vercesi^{70a}, M. Verducci^{71a,71b}, C.M. Vergel Infante⁷⁸, C. Vergis²⁴, W. Verkerke¹²⁰, A.T. Vermeulen¹²⁰,
 J.C. Vermeulen¹²⁰, M.C. Vetterli^{152,ax}, N. Viaux Maira^{147b}, M. Vicente Barreto Pinto⁵⁴, T. Vickey¹⁴⁹,
 O.E. Vickey Boeriu¹⁴⁹, G.H.A. Viehhauser¹³⁵, L. Vigani^{61b}, M. Villa^{23b,23a}, M. Villaplana Perez^{68a,68b},
 E. Vilucchi⁵¹, M.G. Vinciter³⁴, V.B. Vinogradov⁷⁹, A. Vishwakarma⁴⁶, C. Vittori^{23b,23a}, I. Vivarelli¹⁵⁶,

M. Vogel¹⁸², P. Vokac¹⁴², S.E. von Buddenbrock^{33c}, E. Von Toerne²⁴, V. Vorobel¹⁴³, K. Vorobev¹¹², M. Vos¹⁷⁴, J.H. Vosseveld⁹⁰, M. Vozak¹⁰⁰, N. Vranjes¹⁶, M. Vranjes Milosavljevic¹⁶, V. Vrba¹⁴², M. Vreeswijk¹²⁰, T. Šfiligoj⁹¹, R. Vuillermet³⁶, I. Vukotic³⁷, T. Ženiš^{28a}, L. Živković¹⁶, P. Wagner²⁴, W. Wagner¹⁸², J. Wagner-Kuhr¹¹⁴, S. Wahdan¹⁸², H. Wahlberg⁸⁸, K. Wakamiya⁸², V.M. Walbrecht¹¹⁵, J. Walder⁸⁹, R. Walker¹¹⁴, S.D. Walker⁹³, W. Walkowiak¹⁵¹, V. Wallangen^{45a,45b}, A.M. Wang⁵⁹, C. Wang^{60c}, C. Wang^{60b}, F. Wang¹⁸¹, H. Wang¹⁸, H. Wang³, J. Wang¹⁵⁷, J. Wang^{61b}, P. Wang⁴², Q. Wang¹²⁸, R.-J. Wang⁹⁹, R. Wang^{60a}, R. Wang⁶, S.M. Wang¹⁵⁸, W.T. Wang^{60a}, W. Wang^{15c,ae}, W.X. Wang^{60a,ae}, Y. Wang^{60a,am}, Z. Wang^{60c}, C. Wanotayaroj⁴⁶, A. Warburton¹⁰³, C.P. Ward³², D.R. Wardrope⁹⁴, N. Warrack⁵⁷, A. Washbrook⁵⁰, A.T. Watson²¹, M.F. Watson²¹, G. Watts¹⁴⁸, B.M. Waugh⁹⁴, A.F. Webb¹¹, S. Webb⁹⁹, C. Weber¹⁸³, M.S. Weber²⁰, S.A. Weber³⁴, S.M. Weber^{61a}, A.R. Weidberg¹³⁵, J. Weingarten⁴⁷, M. Weirich⁹⁹, C. Weiser⁵², P.S. Wells³⁶, T. Wenaus²⁹, T. Wengler³⁶, S. Wenig³⁶, N. Wermes²⁴, M.D. Werner⁷⁸, M. Wessels^{61a}, T.D. Weston²⁰, K. Whalen¹³¹, N.L. Whallon¹⁴⁸, A.M. Wharton⁸⁹, A.S. White¹⁰⁵, A. White⁸, M.J. White¹, D. Whiteson¹⁷¹, B.W. Whitmore⁸⁹, W. Wiedenmann¹⁸¹, M. Wielers¹⁴⁴, N. Wieseotte⁹⁹, C. Wiglesworth⁴⁰, L.A.M. Wiik-Fuchs⁵², F. Wilk¹⁰⁰, H.G. Wilkens³⁶, L.J. Wilkins⁹³, H.H. Williams¹³⁷, S. Williams³², C. Willis¹⁰⁶, S. Willocq¹⁰², J.A. Wilson²¹, I. Wingerter-Seez⁵, E. Winkels¹⁵⁶, F. Winklmeier¹³¹, O.J. Winston¹⁵⁶, B.T. Winter⁵², M. Wittgen¹⁵³, M. Wobisch⁹⁵, A. Wolf⁹⁹, T.M.H. Wolf¹²⁰, R. Wolff¹⁰¹, R.W. Wölker¹³⁵, J. Wollrath⁵², M.W. Wolter⁸⁴, H. Wolters^{140a,140c}, V.W.S. Wong¹⁷⁵, N.L. Woods¹⁴⁶, S.D. Worm²¹, B.K. Wosiek⁸⁴, K.W. Woźniak⁸⁴, K. Wraight⁵⁷, S.L. Wu¹⁸¹, X. Wu⁵⁴, Y. Wu^{60a}, T.R. Wyatt¹⁰⁰, B.M. Wynne⁵⁰, S. Xella⁴⁰, Z. Xi¹⁰⁵, L. Xia¹⁷⁸, D. Xu^{15a}, H. Xu^{60a,b}, L. Xu²⁹, T. Xu¹⁴⁵, W. Xu¹⁰⁵, Z. Xu^{60b}, Z. Xu¹⁵³, B. Yabsley¹⁵⁷, S. Yacooob^{33a}, K. Yajima¹³³, D.P. Yallup⁹⁴, D. Yamaguchi¹⁶⁵, Y. Yamaguchi¹⁶⁵, A. Yamamoto⁸¹, F. Yamane⁸², M. Yamatani¹⁶³, T. Yamazaki¹⁶³, Y. Yamazaki⁸², Z. Yan²⁵, H.J. Yang^{60c,60d}, H.T. Yang¹⁸, S. Yang⁷⁷, X. Yang^{60b,58}, Y. Yang¹⁶³, W.-M. Yao¹⁸, Y.C. Yap⁴⁶, Y. Yasu⁸¹, E. Yatsenko^{60c,60d}, J. Ye⁴², S. Ye²⁹, I. Yeletsikh⁷⁹, M.R. Yexley⁸⁹, E. Yigitbasi²⁵, K. Yorita¹⁷⁹, K. Yoshihara¹³⁷, C.J.S. Young³⁶, C. Young¹⁵³, J. Yu⁷⁸, R. Yuan^{60b,h}, X. Yue^{61a}, S.P.Y. Yuen²⁴, B. Zabinski⁸⁴, G. Zacharis¹⁰, E. Zaffaroni⁵⁴, J. Zahreddine¹³⁶, A.M. Zaitsev^{123,ao}, T. Zakareishvili^{159b}, N. Zakharchuk³⁴, S. Zambito⁵⁹, D. Zanzi³⁶, D.R. Zaripovas⁵⁷, S.V. Zeiβner⁴⁷, C. Zeitnitz¹⁸², G. Zemaityte¹³⁵, J.C. Zeng¹⁷³, O. Zenin¹²³, D. Zerwas¹³², M. Zgubič¹³⁵, D.F. Zhang^{15b}, F. Zhang¹⁸¹, G. Zhang^{15b}, H. Zhang^{15c}, J. Zhang⁶, L. Zhang^{15c}, L. Zhang^{60a}, M. Zhang¹⁷³, R. Zhang²⁴, X. Zhang^{60b}, Y. Zhang^{15a,15d}, Z. Zhang^{63a}, Z. Zhang¹³², P. Zhao⁴⁹, Y. Zhao^{60b}, Z. Zhao^{60a}, A. Zhemchugov⁷⁹, Z. Zheng¹⁰⁵, D. Zhong¹⁷³, B. Zhou¹⁰⁵, C. Zhou¹⁸¹, M.S. Zhou^{15a,15d}, M. Zhou¹⁵⁵, N. Zhou^{60c}, Y. Zhou⁷, C.G. Zhu^{60b}, H.L. Zhu^{60a}, H. Zhu^{15a}, J. Zhu¹⁰⁵, Y. Zhu^{60a}, X. Zhuang^{15a}, K. Zhukov¹¹⁰, V. Zhulanov^{122b,122a}, D. Ziemska⁶⁵, N.I. Zimine⁷⁹, S. Zimmermann⁵², Z. Zinonos¹¹⁵, M. Ziolkowski¹⁵¹, G. Zoernig¹⁸¹, A. Zoccoli^{23b,23a}, K. Zoch⁵³, T.G. Zorbas¹⁴⁹, R. Zou³⁷ and L. Zwalinski³⁶

¹ Department of Physics, University of Adelaide, Adelaide; Australia

² Physics Department, SUNY Albany, Albany NY; United States of America

³ Department of Physics, University of Alberta, Edmonton AB; Canada

⁴ (a)Department of Physics, Ankara University, Ankara, (b)Istanbul Aydin University, Istanbul, (c)Division of Physics, TOBB University of Economics and Technology, Ankara; Turkey

⁵ LAPP, Université Grenoble Alpes, Université Savoie Mont Blanc, CNRS/IN2P3, Annecy; France

⁶ High Energy Physics Division, Argonne National Laboratory, Argonne IL; United States of America

⁷ Department of Physics, University of Arizona, Tucson AZ; United States of America

⁸ Department of Physics, University of Texas at Arlington, Arlington TX; United States of America

⁹ Physics Department, National and Kapodistrian University of Athens, Athens; Greece

¹⁰ Physics Department, National Technical University of Athens, Zografou; Greece

¹¹ Department of Physics, University of Texas at Austin, Austin TX; United States of America

¹² (a)Bahcesehir University, Faculty of Engineering and Natural Sciences, Istanbul, (b)Istanbul Bilgi University, Faculty of Engineering and Natural Sciences, Istanbul, (c)Department of Physics, Bogazici University, Istanbul, (d)Department of Physics Engineering, Gaziantep University, Gaziantep; Turkey

- 13 *Institute of Physics, Azerbaijan Academy of Sciences, Baku; Azerbaijan*
- 14 *Institut de Física d'Altes Energies (IFAE), Barcelona Institute of Science and Technology, Barcelona; Spain*
- 15 ^(a)*Institute of High Energy Physics, Chinese Academy of Sciences, Beijing;* ^(b)*Physics Department, Tsinghua University, Beijing;* ^(c)*Department of Physics, Nanjing University, Nanjing;* ^(d)*University of Chinese Academy of Science (UCAS), Beijing; China*
- 16 *Institute of Physics, University of Belgrade, Belgrade; Serbia*
- 17 *Department for Physics and Technology, University of Bergen, Bergen; Norway*
- 18 *Physics Division, Lawrence Berkeley National Laboratory and University of California, Berkeley CA; United States of America*
- 19 *Institut für Physik, Humboldt Universität zu Berlin, Berlin; Germany*
- 20 *Albert Einstein Center for Fundamental Physics and Laboratory for High Energy Physics, University of Bern, Bern; Switzerland*
- 21 *School of Physics and Astronomy, University of Birmingham, Birmingham; United Kingdom*
- 22 *Facultad de Ciencias y Centro de Investigaciones, Universidad Antonio Nariño, Bogota; Colombia*
- 23 ^(a)*INFN Bologna and Università di Bologna, Dipartimento di Fisica;* ^(b)*INFN Sezione di Bologna; Italy*
- 24 *Physikalisches Institut, Universität Bonn, Bonn; Germany*
- 25 *Department of Physics, Boston University, Boston MA; United States of America*
- 26 *Department of Physics, Brandeis University, Waltham MA; United States of America*
- 27 ^(a)*Transilvania University of Brasov, Brasov;* ^(b)*Horia Hulubei National Institute of Physics and Nuclear Engineering, Bucharest;* ^(c)*Department of Physics, Alexandru Ioan Cuza University of Iasi, Iasi;* ^(d)*National Institute for Research and Development of Isotopic and Molecular Technologies, Physics Department, Cluj-Napoca;* ^(e)*University Politehnica Bucharest, Bucharest;* ^(f)*West University in Timisoara, Timisoara; Romania*
- 28 ^(a)*Faculty of Mathematics, Physics and Informatics, Comenius University, Bratislava;* ^(b)*Department of Subnuclear Physics, Institute of Experimental Physics of the Slovak Academy of Sciences, Kosice; Slovak Republic*
- 29 *Physics Department, Brookhaven National Laboratory, Upton NY; United States of America*
- 30 *Departamento de Física, Universidad de Buenos Aires, Buenos Aires; Argentina*
- 31 *California State University, CA; United States of America*
- 32 *Cavendish Laboratory, University of Cambridge, Cambridge; United Kingdom*
- 33 ^(a)*Department of Physics, University of Cape Town, Cape Town;* ^(b)*Department of Mechanical Engineering Science, University of Johannesburg, Johannesburg;* ^(c)*School of Physics, University of the Witwatersrand, Johannesburg; South Africa*
- 34 *Department of Physics, Carleton University, Ottawa ON; Canada*
- 35 ^(a)*Faculté des Sciences Ain Chock, Réseau Universitaire de Physique des Hautes Energies — Université Hassan II, Casablanca;* ^(b)*Faculté des Sciences, Université Ibn-Tofail, Kénitra;* ^(c)*Faculté des Sciences Semlalia, Université Cadi Ayyad, LPHEA-Marrakech;* ^(d)*Faculté des Sciences, Université Mohamed Premier and LPTPM, Oujda;* ^(e)*Faculté des sciences, Université Mohammed V, Rabat; Morocco*
- 36 *CERN, Geneva; Switzerland*
- 37 *Enrico Fermi Institute, University of Chicago, Chicago IL; United States of America*
- 38 *LPC, Université Clermont Auvergne, CNRS/IN2P3, Clermont-Ferrand; France*
- 39 *Nevis Laboratory, Columbia University, Irvington NY; United States of America*
- 40 *Niels Bohr Institute, University of Copenhagen, Copenhagen; Denmark*
- 41 ^(a)*Dipartimento di Fisica, Università della Calabria, Rende;* ^(b)*INFN Gruppo Collegato di Cosenza, Laboratori Nazionali di Frascati; Italy*
- 42 *Physics Department, Southern Methodist University, Dallas TX; United States of America*
- 43 *Physics Department, University of Texas at Dallas, Richardson TX; United States of America*
- 44 *National Centre for Scientific Research “Demokritos”, Agia Paraskevi; Greece*
- 45 ^(a)*Department of Physics, Stockholm University;* ^(b)*Oskar Klein Centre, Stockholm; Sweden*
- 46 *Deutsches Elektronen-Synchrotron DESY, Hamburg and Zeuthen; Germany*
- 47 *Lehrstuhl für Experimentelle Physik IV, Technische Universität Dortmund, Dortmund; Germany*
- 48 *Institut für Kern- und Teilchenphysik, Technische Universität Dresden, Dresden; Germany*

- 49 *Department of Physics, Duke University, Durham NC; United States of America*
- 50 *SUPA — School of Physics and Astronomy, University of Edinburgh, Edinburgh; United Kingdom*
- 51 *INFN e Laboratori Nazionali di Frascati, Frascati; Italy*
- 52 *Physikalisches Institut, Albert-Ludwigs-Universität Freiburg, Freiburg; Germany*
- 53 *II. Physikalisches Institut, Georg-August-Universität Göttingen, Göttingen; Germany*
- 54 *Département de Physique Nucléaire et Corpusculaire, Université de Genève, Genève; Switzerland*
- 55 *(a)Dipartimento di Fisica, Università di Genova, Genova;(b)INFN Sezione di Genova; Italy*
- 56 *II. Physikalisches Institut, Justus-Liebig-Universität Giessen, Giessen; Germany*
- 57 *SUPA — School of Physics and Astronomy, University of Glasgow, Glasgow; United Kingdom*
- 58 *LPSC, Université Grenoble Alpes, CNRS/IN2P3, Grenoble INP, Grenoble; France*
- 59 *Laboratory for Particle Physics and Cosmology, Harvard University, Cambridge MA; United States of America*
- 60 *(a)Department of Modern Physics and State Key Laboratory of Particle Detection and Electronics, University of Science and Technology of China, Hefei;(b)Institute of Frontier and Interdisciplinary Science and Key Laboratory of Particle Physics and Particle Irradiation (MOE), Shandong University, Qingdao;(c)School of Physics and Astronomy, Shanghai Jiao Tong University, KLPPAC-MoE, SKLPPC, Shanghai;(d)Tsung-Dao Lee Institute, Shanghai; China*
- 61 *(a)Kirchhoff-Institut für Physik, Ruprecht-Karls-Universität Heidelberg, Heidelberg;(b)Physikalisches Institut, Ruprecht-Karls-Universität Heidelberg, Heidelberg; Germany*
- 62 *Faculty of Applied Information Science, Hiroshima Institute of Technology, Hiroshima; Japan*
- 63 *(a)Department of Physics, Chinese University of Hong Kong, Shatin, N.T., Hong Kong;(b)Department of Physics, University of Hong Kong, Hong Kong;(c)Department of Physics and Institute for Advanced Study, Hong Kong University of Science and Technology, Clear Water Bay, Kowloon, Hong Kong; China*
- 64 *Department of Physics, National Tsing Hua University, Hsinchu; Taiwan*
- 65 *Department of Physics, Indiana University, Bloomington IN; United States of America*
- 66 *(a)INFN Gruppo Collegato di Udine, Sezione di Trieste, Udine;(b)ICTP, Trieste;(c)Dipartimento Politecnico di Ingegneria e Architettura, Università di Udine, Udine; Italy*
- 67 *(a)INFN Sezione di Lecce;(b)Dipartimento di Matematica e Fisica, Università del Salento, Lecce; Italy*
- 68 *(a)INFN Sezione di Milano;(b)Dipartimento di Fisica, Università di Milano, Milano; Italy*
- 69 *(a)INFN Sezione di Napoli;(b)Dipartimento di Fisica, Università di Napoli, Napoli; Italy*
- 70 *(a)INFN Sezione di Pavia;(b)Dipartimento di Fisica, Università di Pavia, Pavia; Italy*
- 71 *(a)INFN Sezione di Pisa;(b)Dipartimento di Fisica E. Fermi, Università di Pisa, Pisa; Italy*
- 72 *(a)INFN Sezione di Roma;(b)Dipartimento di Fisica, Sapienza Università di Roma, Roma; Italy*
- 73 *(a)INFN Sezione di Roma Tor Vergata;(b)Dipartimento di Fisica, Università di Roma Tor Vergata, Roma; Italy*
- 74 *(a)INFN Sezione di Roma Tre;(b)Dipartimento di Matematica e Fisica, Università Roma Tre, Roma; Italy*
- 75 *(a)INFN-TIFPA;(b)Università degli Studi di Trento, Trento; Italy*
- 76 *Institut für Astro- und Teilchenphysik, Leopold-Franzens-Universität, Innsbruck; Austria*
- 77 *University of Iowa, Iowa City IA; United States of America*
- 78 *Department of Physics and Astronomy, Iowa State University, Ames IA; United States of America*
- 79 *Joint Institute for Nuclear Research, Dubna; Russia*
- 80 *(a)Departamento de Engenharia Elétrica, Universidade Federal de Juiz de Fora (UFJF), Juiz de Fora;(b)Universidade Federal do Rio De Janeiro COPPE/EE/IF, Rio de Janeiro;(c)Universidade Federal de São João del Rei (UFSJ), São João del Rei;(d)Instituto de Física, Universidade de São Paulo, São Paulo; Brazil*
- 81 *KEK, High Energy Accelerator Research Organization, Tsukuba; Japan*
- 82 *Graduate School of Science, Kobe University, Kobe; Japan*
- 83 *(a)AGH University of Science and Technology, Faculty of Physics and Applied Computer Science, Krakow;(b)Marian Smoluchowski Institute of Physics, Jagiellonian University, Krakow; Poland*
- 84 *Institute of Nuclear Physics Polish Academy of Sciences, Krakow; Poland*
- 85 *Faculty of Science, Kyoto University, Kyoto; Japan*
- 86 *Kyoto University of Education, Kyoto; Japan*
- 87 *Research Center for Advanced Particle Physics and Department of Physics, Kyushu University, Fukuoka; Japan*
- 88 *Instituto de Física La Plata, Universidad Nacional de La Plata and CONICET, La Plata; Argentina*
- 89 *Physics Department, Lancaster University, Lancaster; United Kingdom*

- 90 *Oliver Lodge Laboratory, University of Liverpool, Liverpool; United Kingdom*
- 91 *Department of Experimental Particle Physics, Jožef Stefan Institute and Department of Physics, University of Ljubljana, Ljubljana; Slovenia*
- 92 *School of Physics and Astronomy, Queen Mary University of London, London; United Kingdom*
- 93 *Department of Physics, Royal Holloway University of London, Egham; United Kingdom*
- 94 *Department of Physics and Astronomy, University College London, London; United Kingdom*
- 95 *Louisiana Tech University, Ruston LA; United States of America*
- 96 *Fysiska institutionen, Lunds universitet, Lund; Sweden*
- 97 *Centre de Calcul de l'Institut National de Physique Nucléaire et de Physique des Particules (IN2P3), Villeurbanne; France*
- 98 *Departamento de Física Teórica C-15 and CIAFF, Universidad Autónoma de Madrid, Madrid; Spain*
- 99 *Institut für Physik, Universität Mainz, Mainz; Germany*
- 100 *School of Physics and Astronomy, University of Manchester, Manchester; United Kingdom*
- 101 *CPPM, Aix-Marseille Université, CNRS/IN2P3, Marseille; France*
- 102 *Department of Physics, University of Massachusetts, Amherst MA; United States of America*
- 103 *Department of Physics, McGill University, Montreal QC; Canada*
- 104 *School of Physics, University of Melbourne, Victoria; Australia*
- 105 *Department of Physics, University of Michigan, Ann Arbor MI; United States of America*
- 106 *Department of Physics and Astronomy, Michigan State University, East Lansing MI; United States of America*
- 107 *B.I. Stepanov Institute of Physics, National Academy of Sciences of Belarus, Minsk; Belarus*
- 108 *Research Institute for Nuclear Problems of Byelorussian State University, Minsk; Belarus*
- 109 *Group of Particle Physics, University of Montreal, Montreal QC; Canada*
- 110 *P.N. Lebedev Physical Institute of the Russian Academy of Sciences, Moscow; Russia*
- 111 *Institute for Theoretical and Experimental Physics of the National Research Centre Kurchatov Institute, Moscow; Russia*
- 112 *National Research Nuclear University MEPhI, Moscow; Russia*
- 113 *D.V. Skobeltsyn Institute of Nuclear Physics, M.V. Lomonosov Moscow State University, Moscow; Russia*
- 114 *Fakultät für Physik, Ludwig-Maximilians-Universität München, München; Germany*
- 115 *Max-Planck-Institut für Physik (Werner-Heisenberg-Institut), München; Germany*
- 116 *Nagasaki Institute of Applied Science, Nagasaki; Japan*
- 117 *Graduate School of Science and Kobayashi-Maskawa Institute, Nagoya University, Nagoya; Japan*
- 118 *Department of Physics and Astronomy, University of New Mexico, Albuquerque NM; United States of America*
- 119 *Institute for Mathematics, Astrophysics and Particle Physics, Radboud University Nijmegen/Nikhef, Nijmegen; Netherlands*
- 120 *Nikhef National Institute for Subatomic Physics and University of Amsterdam, Amsterdam; Netherlands*
- 121 *Department of Physics, Northern Illinois University, DeKalb IL; United States of America*
- 122 *(a) Budker Institute of Nuclear Physics and NSU, SB RAS, Novosibirsk; (b) Novosibirsk State University Novosibirsk; Russia*
- 123 *Institute for High Energy Physics of the National Research Centre Kurchatov Institute, Protvino; Russia*
- 124 *Department of Physics, New York University, New York NY; United States of America*
- 125 *Ochanomizu University, Otsuka, Bunkyo-ku, Tokyo; Japan*
- 126 *Ohio State University, Columbus OH; United States of America*
- 127 *Faculty of Science, Okayama University, Okayama; Japan*
- 128 *Homer L. Dodge Department of Physics and Astronomy, University of Oklahoma, Norman OK; United States of America*
- 129 *Department of Physics, Oklahoma State University, Stillwater OK; United States of America*
- 130 *Palacký University, RCPTM, Joint Laboratory of Optics, Olomouc; Czech Republic*
- 131 *Center for High Energy Physics, University of Oregon, Eugene OR; United States of America*
- 132 *LAL, Université Paris-Sud, CNRS/IN2P3, Université Paris-Saclay, Orsay; France*
- 133 *Graduate School of Science, Osaka University, Osaka; Japan*
- 134 *Department of Physics, University of Oslo, Oslo; Norway*
- 135 *Department of Physics, Oxford University, Oxford; United Kingdom*

- 136 LPNHE, Sorbonne Université, Paris Diderot Sorbonne Paris Cité, CNRS/IN2P3, Paris; France
 137 Department of Physics, University of Pennsylvania, Philadelphia PA; United States of America
 138 Konstantinov Nuclear Physics Institute of National Research Centre “Kurchatov Institute”, PNPI, St. Petersburg; Russia
 139 Department of Physics and Astronomy, University of Pittsburgh, Pittsburgh PA; United States of America
 140 (a) Laboratório de Instrumentação e Física Experimental de Partículas — LIP; (b) Departamento de Física, Faculdade de Ciências, Universidade de Lisboa, Lisboa; (c) Departamento de Física, Universidade de Coimbra, Coimbra; (d) Centro de Física Nuclear da Universidade de Lisboa, Lisboa; (e) Departamento de Física, Universidade do Minho, Braga; (f) Universidad de Granada, Granada (Spain); (g) Dep Física and CEFITEC of Faculdade de Ciências e Tecnologia, Universidade Nova de Lisboa, Caparica; (h) Av. Rovisco Pais, 1 1049-001 Lisbon, Portugal; Portugal
 141 Institute of Physics of the Czech Academy of Sciences, Prague; Czech Republic
 142 Czech Technical University in Prague, Prague; Czech Republic
 143 Charles University, Faculty of Mathematics and Physics, Prague; Czech Republic
 144 Particle Physics Department, Rutherford Appleton Laboratory, Didcot; United Kingdom
 145 IRFU, CEA, Université Paris-Saclay, Gif-sur-Yvette; France
 146 Santa Cruz Institute for Particle Physics, University of California Santa Cruz, Santa Cruz CA; United States of America
 147 (a) Departamento de Física, Pontificia Universidad Católica de Chile, Santiago; (b) Departamento de Física, Universidad Técnica Federico Santa María, Valparaíso; Chile
 148 Department of Physics, University of Washington, Seattle WA; United States of America
 149 Department of Physics and Astronomy, University of Sheffield, Sheffield; United Kingdom
 150 Department of Physics, Shinshu University, Nagano; Japan
 151 Department Physik, Universität Siegen, Siegen; Germany
 152 Department of Physics, Simon Fraser University, Burnaby BC; Canada
 153 SLAC National Accelerator Laboratory, Stanford CA; United States of America
 154 Physics Department, Royal Institute of Technology, Stockholm; Sweden
 155 Departments of Physics and Astronomy, Stony Brook University, Stony Brook NY; United States of America
 156 Department of Physics and Astronomy, University of Sussex, Brighton; United Kingdom
 157 School of Physics, University of Sydney, Sydney; Australia
 158 Institute of Physics, Academia Sinica, Taipei; Taiwan
 159 (a) E. Andronikashvili Institute of Physics, Iv. Javakishvili Tbilisi State University, Tbilisi; (b) High Energy Physics Institute, Tbilisi State University, Tbilisi; Georgia
 160 Department of Physics, Technion, Israel Institute of Technology, Haifa; Israel
 161 Raymond and Beverly Sackler School of Physics and Astronomy, Tel Aviv University, Tel Aviv; Israel
 162 Department of Physics, Aristotle University of Thessaloniki, Thessaloniki; Greece
 163 International Center for Elementary Particle Physics and Department of Physics, University of Tokyo, Tokyo; Japan
 164 Graduate School of Science and Technology, Tokyo Metropolitan University, Tokyo; Japan
 165 Department of Physics, Tokyo Institute of Technology, Tokyo; Japan
 166 Tomsk State University, Tomsk; Russia
 167 Department of Physics, University of Toronto, Toronto ON; Canada
 168 (a) TRIUMF, Vancouver BC; (b) Department of Physics and Astronomy, York University, Toronto ON; Canada
 169 Division of Physics and Tomonaga Center for the History of the Universe, Faculty of Pure and Applied Sciences, University of Tsukuba, Tsukuba; Japan
 170 Department of Physics and Astronomy, Tufts University, Medford MA; United States of America
 171 Department of Physics and Astronomy, University of California Irvine, Irvine CA; United States of America
 172 Department of Physics and Astronomy, University of Uppsala, Uppsala; Sweden
 173 Department of Physics, University of Illinois, Urbana IL; United States of America
 174 Instituto de Física Corpuscular (IFIC), Centro Mixto Universidad de Valencia — CSIC, Valencia; Spain
 175 Department of Physics, University of British Columbia, Vancouver BC; Canada
 176 Department of Physics and Astronomy, University of Victoria, Victoria BC; Canada

- 177 *Fakultät für Physik und Astronomie, Julius-Maximilians-Universität Würzburg, Würzburg; Germany*
 178 *Department of Physics, University of Warwick, Coventry; United Kingdom*
 179 *Waseda University, Tokyo; Japan*
 180 *Department of Particle Physics, Weizmann Institute of Science, Rehovot; Israel*
 181 *Department of Physics, University of Wisconsin, Madison WI; United States of America*
 182 *Fakultät für Mathematik und Naturwissenschaften, Fachgruppe Physik, Bergische Universität Wuppertal, Wuppertal; Germany*
 183 *Department of Physics, Yale University, New Haven CT; United States of America*
 184 *Yerevan Physics Institute, Yerevan; Armenia*
- a Also at CERN, Geneva; Switzerland*
b Also at CPPM, Aix-Marseille Université, CNRS/IN2P3, Marseille; France
c Also at Département de Physique Nucléaire et Corpusculaire, Université de Genève, Genève; Switzerland
d Also at Departament de Física de la Universitat Autònoma de Barcelona, Barcelona; Spain
e Also at Departamento de Física, Instituto Superior Técnico, Universidade de Lisboa, Lisboa; Portugal
f Also at Department of Applied Physics and Astronomy, University of Sharjah, Sharjah; United Arab Emirates
g Also at Department of Financial and Management Engineering, University of the Aegean, Chios; Greece
h Also at Department of Physics and Astronomy, Michigan State University, East Lansing MI; United States of America
i Also at Department of Physics and Astronomy, University of Louisville, Louisville, KY; United States of America
j Also at Department of Physics and Astronomy, University of Sheffield, Sheffield; United Kingdom
k Also at Department of Physics, California State University, East Bay; United States of America
l Also at Department of Physics, California State University, Fresno; United States of America
m Also at Department of Physics, California State University, Sacramento; United States of America
n Also at Department of Physics, King's College London, London; United Kingdom
o Also at Department of Physics, St. Petersburg State Polytechnical University, St. Petersburg; Russia
p Also at Department of Physics, Stanford University, Stanford CA; United States of America
q Also at Department of Physics, University of Adelaide, Adelaide; Australia
r Also at Department of Physics, University of Fribourg, Fribourg; Switzerland
s Also at Department of Physics, University of Michigan, Ann Arbor MI; United States of America
t Also at Faculty of Physics, M.V. Lomonosov Moscow State University, Moscow; Russia
u Also at Giresun University, Faculty of Engineering, Giresun; Turkey
v Also at Graduate School of Science, Osaka University, Osaka; Japan
w Also at Hellenic Open University, Patras; Greece
x Also at Institutio Catalana de Recerca i Estudis Avancats, ICREA, Barcelona; Spain
y Also at Institut für Experimentalphysik, Universität Hamburg, Hamburg; Germany
z Also at Institute for Mathematics, Astrophysics and Particle Physics, Radboud University Nijmegen/Nikhef, Nijmegen; Netherlands
- aa Also at Institute for Nuclear Research and Nuclear Energy (INRNE) of the Bulgarian Academy of Sciences, Sofia; Bulgaria*
ab Also at Institute for Particle and Nuclear Physics, Wigner Research Centre for Physics, Budapest; Hungary
ac Also at Institute of High Energy Physics, Chinese Academy of Sciences, Beijing; China
ad Also at Institute of Particle Physics (IPP); Canada
ae Also at Institute of Physics, Academia Sinica, Taipei; Taiwan
af Also at Institute of Physics, Azerbaijan Academy of Sciences, Baku; Azerbaijan
ag Also at Institute of Theoretical Physics, Ilia State University, Tbilisi; Georgia
ah Also at Instituto de Física Teórica, IFT-UAM/CSIC, Madrid; Spain
ai Also at Istanbul University, Dept. of Physics, Istanbul; Turkey
aj Also at Joint Institute for Nuclear Research, Dubna; Russia
ak Also at LAL, Université Paris-Sud, CNRS/IN2P3, Université Paris-Saclay, Orsay; France
al Also at Louisiana Tech University, Ruston LA; United States of America
am Also at LPNHE, Sorbonne Université, Paris Diderot Sorbonne Paris Cité, CNRS/IN2P3, Paris; France

- an* Also at Manhattan College, New York NY; United States of America
ao Also at Moscow Institute of Physics and Technology State University, Dolgoprudny; Russia
ap Also at National Research Nuclear University MEPhI, Moscow; Russia
aq Also at Physics Department, An-Najah National University, Nablus; Palestine
ar Also at Physics Dept, University of South Africa, Pretoria; South Africa
as Also at Physikalisches Institut, Albert-Ludwigs-Universität Freiburg, Freiburg; Germany
at Also at School of Physics, Sun Yat-sen University, Guangzhou; China
au Also at The City College of New York, New York NY; United States of America
av Also at The Collaborative Innovation Center of Quantum Matter (CICQM), Beijing; China
aw Also at Tomsk State University, Tomsk, and Moscow Institute of Physics and Technology State University, Dolgoprudny; Russia
ax Also at TRIUMF, Vancouver BC; Canada
ay Also at Università di Napoli Parthenope, Napoli; Italy
* Deceased